

# Effects of neonatal deafness on resting-state functional network connectivity



Daniel Stolzberg<sup>a,b,\*</sup>, Blake E. Butler<sup>a,b,c</sup>, Stephen G. Lomber<sup>a,b,c,d,\*\*</sup>

<sup>a</sup> Department of Physiology and Pharmacology, University of Western Ontario, London, Ontario, N6A 5C1, Canada

<sup>b</sup> Brain and Mind Institute, University of Western Ontario, London, Ontario, N6A 5B7, Canada

<sup>c</sup> Department of Psychology, University of Western Ontario, London, Ontario, N6A 5C2, Canada

<sup>d</sup> National Centre for Audiology, University of Western Ontario, London, Ontario, N6G 1H1, Canada

## ARTICLE INFO

### Keywords:

Resting-state

fMRI

Functional network connectivity

Hearing

Deafness

Cat

## ABSTRACT

Normal brain development depends on early sensory experience. Behavioral consequences of brain maturation in the absence of sensory input early in life are well documented. For example, experiments with mature, neonatally deaf human or animal subjects have revealed improved peripheral visual motion detection and spatial localization abilities. Such supranormal behavioral abilities in the nondeprived sensory modality are evidence of compensatory plasticity occurring in deprived brain regions at some point or throughout development. Sensory deprived brain regions may simply become unused neural real-estate resulting in a loss of function. Compensatory plasticity and loss of function are likely reflected in the differences in correlations between brain networks in deaf compared with hearing subjects. To address this, we used resting-state functional magnetic resonance imaging (fMRI) in lightly anesthetized hearing and neonatally deafened cats. Group independent component analysis (ICA) was used to identify 20 spatially distinct brain networks across all animals including auditory, visual, somatosensory, cingulate, insular, cerebellar, and subcortical networks. The resulting group ICA components were back-reconstructed to individual animal brains. The maximum correlations between the time-courses associated with each spatial component were computed using functional network connectivity (FNC). While no significant differences in the delay to peak correlations were identified between hearing and deaf cats, we observed 10 (of 190) significant differences in the amplitudes of between-network correlations. Six of the significant differences involved auditory-related networks and four involved visual, cingulate, or somatosensory networks. The results are discussed in context of known behavioral, electrophysiological, and anatomical differences following neonatal deafness. Furthermore, these results identify novel targets for future investigations at the neuronal level.

## Introduction

Development in the absence of a sense alters the maturational trajectory of anatomical and functional connectivity in the brain. The precise nature of functional brain network maturation following early life sensory loss is unclear. Brain development in the absence of a sense has been hypothesized to result in a general reduction of function in corresponding brain regions (i.e. loss of function in auditory cortex in deafness). Functional brain networks may also respond to early life sensory loss in a compensatory manner through the reapportionment of neural tissue to the processing of specific features of another sensory modality. A consequence of compensatory plasticity is that it provides for specific gains in functional processing in one or multiple non-deprived senses.

Gains in function of non-deprived senses have indeed been observed in both animals (Lomber et al., 2010) and humans (Bavelier et al., 2001; Bavelier and Neville, 2002; Bola et al., 2017; Shiell et al., 2014).

Behavioral studies in congenitally deaf cats have identified specific auditory structures that subserve improved visual processing (Lomber et al., 2010). While congenitally deaf cats have been shown to better localize visual stimuli in the periphery than normal hearing animals, this advantage is lost following temporary deactivation of the posterior auditory field (PAF) (Lomber et al., 2010). Deactivation of PAF, however, had no effects on many other aspects of visual processing indicating a specific localization of function. In the same study, temporarily deactivating the dorsal zone of auditory cortex (DZ) of congenitally deaf cats normalized their lower (better) visual motion detection threshold.

**Abbreviations:** FNC, Functional Network Connectivity; ICA, Independent Component Analysis; fMRI, Functional Magnetic Resonance Imaging; GLM, General Linear Model; ABR, Auditory Brainstem Response.

\* Corresponding author. Center for Neural Science, 4 Washington Place, New York University, New York, NY, 10003, USA.

\*\* Corresponding author. Department of Physiology and Pharmacology, University of Western Ontario, London, Ontario, N6A 5C1, Canada.

E-mail addresses: [dstolzbe@uwo.ca](mailto:dstolzbe@uwo.ca) (D. Stolzberg), [steve.lomber@uwo.ca](mailto:steve.lomber@uwo.ca) (S.G. Lomber).

<https://doi.org/10.1016/j.neuroimage.2017.10.002>

Received 1 May 2017; Accepted 2 October 2017

Available online 6 October 2017

1053-8119/© 2017 Elsevier Inc. All rights reserved.

Enhancements in sensory processing were demonstrated to be restricted to specific features of the intact modality, improved visual motion or peripheral spatial localization, supporting evidence for compensatory plasticity in these circumscribed auditory brain regions.

Several studies have sought to identify putative anatomical substrates for the behavioral differences identified in deaf cats (Barone et al., 2013; Butler et al., 2016a; Chabot et al., 2015; Kok et al., 2014). Butler et al. (2016a) identified altered projections to PAF from other auditory, somatosensory, visual, and limbic areas in early deaf compared with hearing cats. In a similar investigation into DZ of deaf cats, Kok et al. (2014) identified a significant decrease in projections from visually responsive areas of the anterior lateral bank of the suprasylvian sulcus (ALLS) and an increase in projections from the posterior lateral bank of the suprasylvian sulcus (PLLS) relative to hearing animals. Changes in anatomical projections following deafness occurring early life are likely to have significant consequences on the functional interactions between auditory and non-auditory regions.

At rest (disengaged from a task), intrinsic correlations in neural activity are observed between various brain regions. Inter-regional correlations group the brain into dynamic, spatially and temporally organized groups of networks (Raichle et al., 2001). Functionally connected resting-state brain networks are constrained by the anatomical connectivity of the brain (Greicius et al., 2009). The effects of compensatory plasticity or loss of function following sensory-deprived maturation should be reflected in differences in functional connectivity between brain networks localized to sensory or non-sensory systems.

Decreases in temporally correlated activity between two brain regions or networks following early sensory loss may be interpreted as a general loss of function involving at least those regions or networks. In contrast, increased temporal correlation may represent a form of compensatory plasticity underlying behaviorally relevant recruitment of brain regions or networks for improved sensory processing. Indeed, in blind subjects who lost their visual abilities early in life, both increases and decreases in functional connectivity were measured relative to sighted individuals suggesting that both functional loss and compensatory plasticity occur in the same brain (Liu et al., 2007).

Here we report the results of using ultra-high field fMRI to identify differences in functional connectivity between brain networks in normal hearing and neonatally deafened cats under light anesthesia. Intrinsic brain networks were identified using the model-free group independent component analysis (ICA). Several of these networks share strong similarities with networks previously identified in humans and other mammals. Functional network correlation (FNC) was used to identify differences in correlations between brain networks in hearing and deaf cats. The results support the idea that signs of both general loss of function as well as compensatory plasticity occur following early sensory loss.

## Methods

### Animals

Twenty cats were examined in this study; 11 hearing and 9 deaf cats. All deafened cats were born to one of three queens in the vivarium located at the University of Western Ontario. Mature hearing cats and pregnant queens were acquired from Liberty Laboratories (Waverly, NY). All procedures were approved by the University of Western Ontario's Animal Use Subcommittee of the University Council on Animal Care and were in accordance with the guidelines specified by the Canadian Council on Animal Care.

### Deafening procedures

Nine cats were deafened within the first month of life (confirmed deaf by P31) using one of two pharmacological protocols, each designed to induce permanent threshold shifts (see Fig. 1A for timeline of hearing for

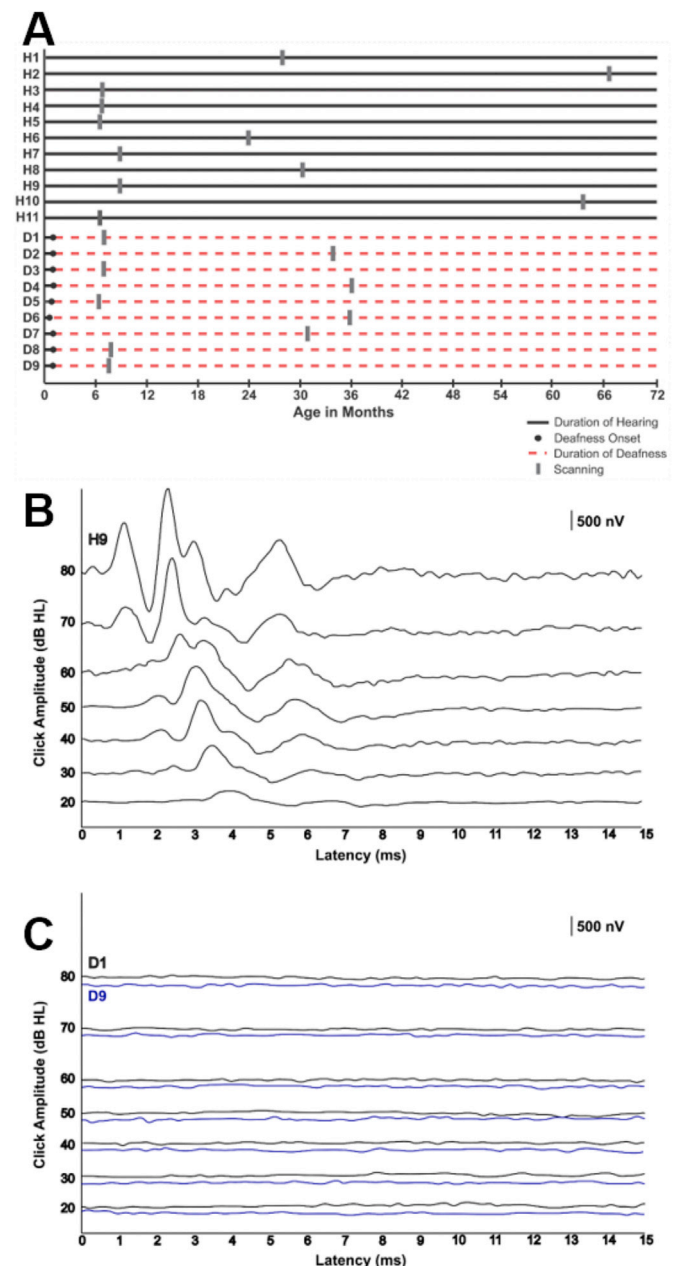


**Fig. 1. Timeline of resting-state scans and hearing status.** A. Timeline of resting-state scans and hearing status. Cats were normal hearing (H) or deafened (D) prior to P31. Example click-evoked auditory brainstem response from a hearing subject (B) and two deaf subjects (overlaid in C). Note that two different deafening procedures were used (see section 2.2 Deafening Procedures). Subject D1 (C, black line) and D9 (C, blue line) serve as examples from each of these two procedures. Click amplitude unit is in hearing level (HL); 80 dB HL is approximately 110 dB SPL for click stimuli.

all animals). Animals D3, D5, D8, and D9 were deafened via daily subcutaneous injections of neomycin (60 mg/kg) beginning at postnatal day one, and ending when no auditory brainstem response (ABR) was observed in response to 80 dB HL (~110 dB SPL) click stimuli (0.1 ms square waves) (Leake et al., 1991). ABR stimuli were presented through ER3A foam insert earbuds (Etymotic Research, Elk Grove Village, IL), and responses were measured using low-impedance subdermal electrodes behind the ears, at the vertex (reference) and at the lower back (ground). The remaining animals (D1, D2, D4, D6, D7) received a single subcutaneous injection of kanamycin (300 mg/kg) combined with an intravenous infusion of ethacrynic acid (35–60 mg/kg to effect) administered via catheter in the cephalic vein of the forelimb (Xu et al., 1993). Animals were anesthetized with isoflurane for the duration of the procedure (5%

to effect for induction; 1–2% for maintenance), and ABRs were recorded continuously using the parameters described above until no response was observed at 80 dB HL (Fig. 1C). At this point, the infusion of ethacrynic acid was discontinued, an infusion of lactated Ringer's solution (4 mL/kg) was provided, the indwelling catheter was removed, and animals were recovered from anesthesia. ABRs were also obtained from all hearing cats prior to functional imaging (Fig. 1B).

#### Image acquisition

Twenty mature cats (deaf  $n = 9$ , female  $n = 4$ , age at scan mean  $\pm$  sem =  $585 \pm 145$  d; hearing  $n = 11$ , female  $n = 7$ , age at scan =  $716 \pm 208$  d; two-tailed independent  $t$ -test comparing age at scan  $t(18) = 0.49$ ,  $p = 0.63$ ) were anesthetised according to a protocol previously established to permit robust haemodynamic response to sound stimuli (Brown et al., 2013; Hall et al., 2014). Prior to each imaging session, cats were pre-medicated with a mixture of atropine (0.02 mg/kg s.c.) and acepromazine (0.02 mg/kg s.c.), then anesthetized approximately 30 min later with a solution of ketamine (4 mg/kg i.m.) and Dexdomitor (0.025–0.05 mg/kg i.m.). Upon confirmation of an absent gag reflex, the animal was intubated and an indwelling catheter was placed in the saphenous vein to facilitate intravenous delivery of fluids and anesthesia. Once prepared, the animal was placed in a sternal position within a custom-built apparatus. Anesthesia was maintained during each session with ketamine (1.2–1.8 mg/kg/h i.v.) and isoflurane (structural imaging  $\approx 0.5\%$ ; functional imaging  $\approx 0.2\%$ – $0.35\%$ ). Resting state functional imaging sessions – when no stimuli were presented to the animal – lasted 10 min and were performed twice per subject. Anesthetised cat body temperature was maintained near normal ( $\sim 38$  C) using heated wax discs and bubble wrap. Anesthetic depth during scanning was assessed using an end-tidal carbon-dioxide (ETCO<sub>2</sub>) monitor and an MRI-compatible pulse-oximeter on a small shaved portion of the animal's tail or foot. Respiration rate, ETCO<sub>2</sub>, pulse rate and oximetry were observed to be stable during imaging sessions. Functional imaging commenced once physiological measures were observed to be stable. Structural scans were performed prior to acquisition of functional data.

Structural and functional MRIs were taken using a 7 TS Magnetom MRI human head-only scanner (68 cm bore diameter) operating at a 350 mT/m/s slew rate and a custom manufactured 8-channel radio-frequency transceive coil was used (Gilbert et al., 2016). B<sub>0</sub> shimming was performed to optimize the magnetic field using an automated 3D mapping procedure (Klassen and Menon, 2004). A high-resolution structural T1-weighted MP2RAGE image was acquired for each subject prior to collecting functional data (repetition time [TR] = 6500 ms, echo time [TE] = 3.93 ms, flip angle 1 = 4°, flip angle 2 = 5°, 96 slices, voxel size = 0.5 mm isotropic). Two 600 s sessions of functional resting state scans were collected using a gradient echo-planar imaging (EPI) sequence with GRAPPA acceleration factor of 2 in axial orientation (TR = 1000 ms, TE = 18 ms, flip angle = 40°, 36 slices, voxel size = 1.0 mm isotropic).

#### Image preprocessing

Brains were manually extracted from structural images. Structural images (T1 scans) were then normalized to an average cat T1 volume and segmented into gray matter, white matter, and cerebral spinal fluid using tissue probability maps (Stolzberg et al., 2017) using the DARTEL toolbox (Ashburner, 2007) for SPM12 (Penny et al., 2011). Initial preprocessing was performed within a single-subject general linear model (GLM) using the CONN toolbox (Whitfield-Gabrieli and Nieto-Castanon, 2012) for Matlab. Functional images were realigned within each session using a 6 degrees-of-freedom rigid-body affine transformation to the session mean functional image and the motion estimates were used as nuisance regressors in the GLM. Realigned functional images were coregistered with the corresponding T1 structural volume. Flow fields created for the structural images during the normalization process were applied to the

coregistered functional images. Normalized functional volumes were spatially smoothed using a three-dimensional Gaussian with a full width at half maximum of 2 mm isotropic.

Physiological noise was reduced for each functional session using the anatomical CompCor approach (Behzadi et al., 2007; Chai et al., 2012). Briefly, the five major principle components of segmented, partial volume corrected (using erosion), white matter and cerebrospinal fluid masks were used as nuisance regressors in the GLM. The functional time series data was filtered simultaneously with the regression step (band-pass frequency corners: 0.008 Hz–0.15 Hz). Histograms of whole-brain voxel-voxel correlations were confirmed to follow a normal distribution with a mean near zero after denoising.

#### Group independent component analysis

Two preprocessed 600 s resting state sessions for each subject were used for spatial group ICA using the GIFT toolbox v4.0a for Matlab (Calhoun et al., 2001; <http://mialab.mrn.org/software/gift/>). ICA requires a predetermined maximum number of signals composing the final signal. We chose this maximal number of components to be 20, typical of similar resting state fMRI studies (Hutchison et al., 2011), since a higher number of components resulted in increasing numbers of fragmented spatial networks which were unlikely to be interpretable as physiologically meaningful. Next, two data reduction steps were used to reduce the computational load prior to running ICA (Calhoun et al., 2001). In the first step, data was reduced to the 30 largest principle components. In the second data reduction step, the grouped data was reduced from 1 200 to 20 principle components (see Fig. 2 for a general schematic of the analysis pipeline).

Group ICA was applied to the reduced preprocessed resting state data using the extended Infomax algorithm (Lee et al., 1999). Resulting independent component networks were judged to be reliable estimates of the true hidden spatial networks after 20 randomly seeded runs of ICA using the *Icasso* procedure (Himberg and Hyvarinen, 2003). Spatial network components were converted to z-scores and threshold at 2 standard deviations (Fig. 3).

Group components were back-reconstructed to the individual subjects using the group ICA (GICA) approach resulting in subject-specific spatial maps and time courses (Calhoun et al., 2001). Time courses for each network were converted to z-scores and used for FNC analysis (see

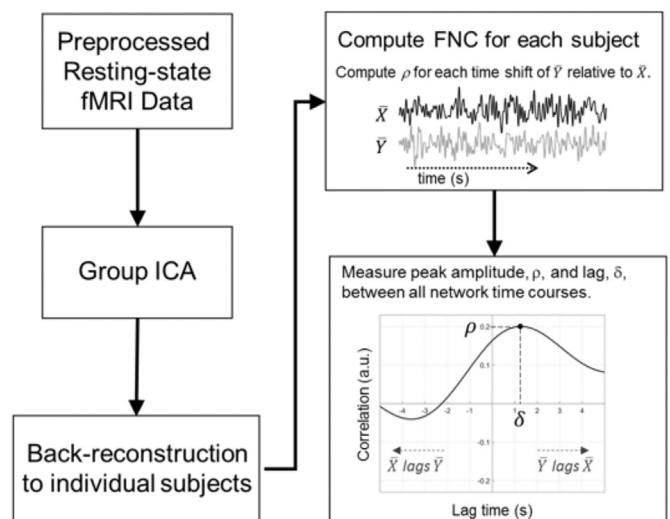


**Fig. 2. Schematic of preprocessing and analysis methods.** Functional network connectivity (FNC) was used to compare the temporal dynamics of independent component network time courses (see section 2.7 for details). Two measures were extracted from the FNC analysis: peak amplitude ( $\rho$ ) and peak lag ( $\delta$ ). A negative value for  $\rho$  is considered an anticorrelation. If  $\delta$  is positive, then the shifted time course,  $\tilde{Y}$ , lags the stationary time course,  $\tilde{X}$ . If  $\delta$  is negative, then  $\tilde{X}$  lags  $\tilde{Y}$ .

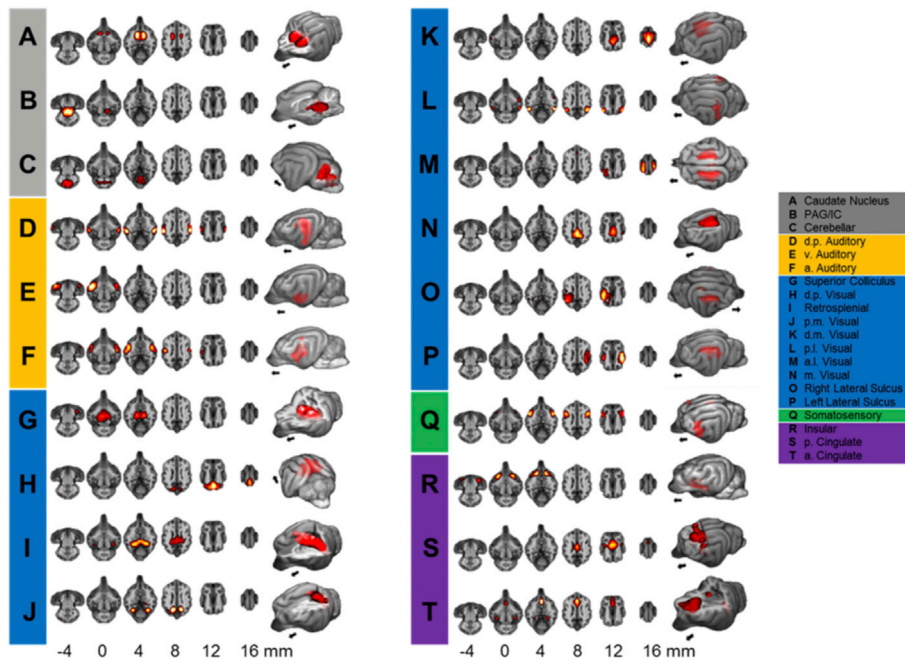


**Fig. 3. Group spatial independent components.** Each of the 20 components are presented as red to yellow z-score maps overlaid on axial slices of an average cat T1 brain. Axial coordinates below each column are relative to the bicomissural plane. Volumetric renderings of the average brain display components as red (z-score > 2) on the brain surface or as volumes within a cutaway section of the brain. Black arrows indicate the anterior direction of each brain. Components are organized into 5 groups (see Fig. 4) indicated by color: Non-Cortical (A-C, gray), Auditory (D-F, yellow), Visual (G-P, blue), Somatosensory (Q, green), Cingulate/Insular (R-T, purple).

section 2.7).

#### Identification of networks

The extents of independent components were evaluated by calculating the percentage of each brain region containing voxels that surpassed threshold (z-score > 2) on a volumetric atlas of the cat cerebral cortex (Stolzberg et al., 2017) and within several additional subcortical structures including the caudate nucleus, inferior colliculus, superior colliculus, periaqueductal gray, and the hippocampus based on Berman and Jones (1982); unlike the cortical structures, subcortical structures were not separated by hemisphere (Fig. 4). The median z-score for each brain region is plotted as a heat map in Fig. 4. The proportion of voxels with z-scores that surpassed a threshold of 2 for each brain region is shown in Supplementary Fig. 1.

#### Functional network connectivity

While spatial ICA minimizes the spatial correlation of the data, temporal relationships between these component time courses may be significantly correlated. Jafri et al. (2008) introduced a measure of functional network connectivity (FNC) to assess the temporal dependencies between the time courses of spatially independent brain networks.

We used FNC to identify temporal relationships between all 20 networks. A total of  $20!/(2!(20-2)!) = 190$  network time course comparisons were performed per subject. Prior to computing FNC, the time courses for each subject were interpolated four times (to 0.25 s resolution). Briefly, the correlation measure,  $\rho$ , is computed between the time course ( $N \times 1$  vector, where  $N$  is the number of samples in each time course) of one network,  $X'$ , and that of a second network  $Y'$ , using the following equation:

$$\rho_{\Delta i} = \frac{(X'^T_{i_0})(Y'_{i_0+\Delta i})}{\sqrt{(X'^T_{i_0}X'_{i_0})} \times \sqrt{(Y'^T_{i_0+\Delta i}Y'_{i_0+\Delta i})}}$$

Here,  $i_0$  is defined as the original time courses and  $i_0 + \Delta i$  defines the shift in signal  $Y'$  relative to its original position. The correlation value,  $\rho_{\Delta i}$ , is computed for each shift of signal  $Y'$ . This procedure is repeated until  $Y'$  is shifted a maximum  $\Delta i = -5$  to  $5$  s (0.25 s steps), resulting in a vector of correlations,  $\rho'_{\Delta i}$ . The absolute largest value from  $\rho'_{\Delta i}$  was selected from each inter-network comparison. The signed amplitude, from here on referred to as  $\rho$ , and the lag to the peak correlation, referred to as  $\delta$ , were collected for comparisons between all networks for each subject (see Fig. 2).

#### Statistics

The Fisher r-to-z transform,  $z = 0.5 \times \ln[(1+r)/(1-r)]$ , was applied to  $\rho$  prior to hypothesis tests to stabilize the sample variance. Estimates of the empirical cumulative distribution functions were generated for the mean between-group differences, (deaf - hearing), separately for the  $\rho$  (amplitude) and  $\delta$  (lag), using a bootstrap procedure (10,000 repetitions). For between-group comparisons, the p-value for zero (i.e., no difference exists between groups) was estimated from the empirical cumulative distributions of between-group differences and were determined to be significant for  $p < 0.05$  after correction using false-discover rate (FDR).

Within-group tests were also performed to determine if peak correlation amplitudes,  $\rho$ , were significantly different from the null hypothesis of no correlation ( $\rho = 0$ ). The bootstrap procedure (10,000 repetitions) was again used to generate an estimate of mean empirical cumulative distribution functions for each of the 190 time course comparisons for each group. P-values supporting the null hypothesis (i.e. no correlation) were determined and within-group values for  $\rho$  were considered significant if  $p_{FDR} < 0.01$ .

Effect sizes were calculated for between-group differences using Hedges'  $g = (M_D - M_H) / SD_{pooled}$ , where  $M$  is the group sample mean and  $SD_{pooled}$  is the pooled weighted within-group standard deviation (Hedges, 1981). Effect size for within-group comparisons were also calculated using Hedges'  $g$  for a single sample comparison,  $g_1 = M/SD$  (Hedges, 1981).

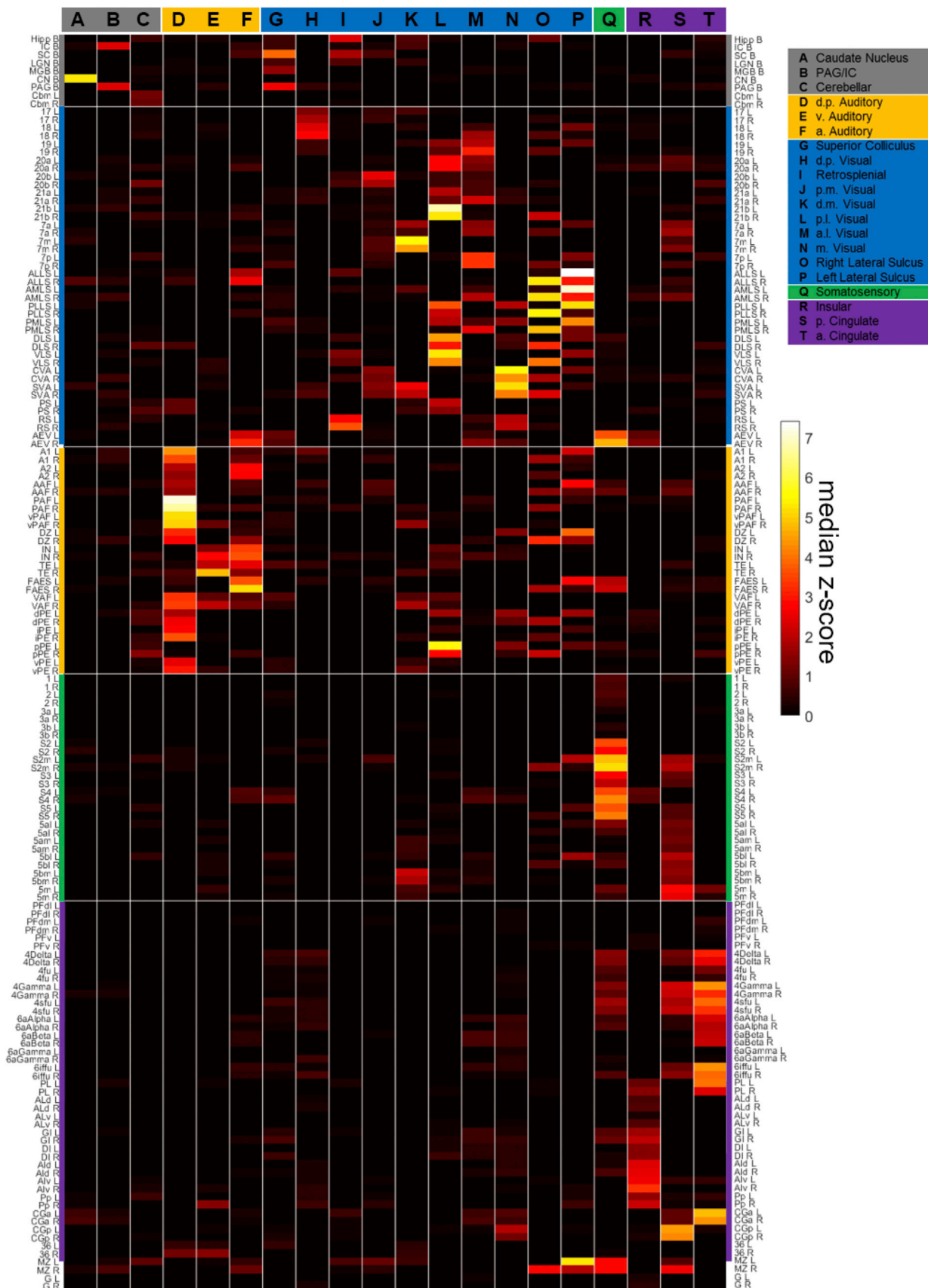


**Fig. 4. Anatomical localization of group independent spatial components.** The heatmap displays the median z-score of each spatial component for each brain region according to the cat brain atlas (Stolzberg et al., 2017). Each region represented in the atlas is displayed redundantly on the left and right of the heatmap. All cortical regions are split by hemisphere (L: Left, R: Right). Subcortical components are represented bilaterally (B). See also Supplementary Fig. 1. See Table 1 for a list of anatomical abbreviations.

## Results

### Deafening and hearing assessment

Two pharmacological methods were used to deafen cats within the first postnatal month (all confirmed deaf by P31, see section 2.1; Fig. 1A). The state of hearing was assessed for all animals using click-evoked auditory brainstem responses (Fig. 1B and C). There was no significant difference in the date of confirmed deafening between the two methods (chronic procedure mean  $\pm$  sem = 24.2  $\pm$  2.4 d; acute procedure = 29.25  $\pm$  1.0 d; two-tailed independent *t*-test:  $t(7) = 1.76$ ,  $p = 0.12$ ; all deaf cats mean  $\pm$  sem = 26.4  $\pm$  1.6 d). Furthermore, a multiple factor analysis of variance (MANOVA) with repeated measures revealed that there was no difference between the two deafening procedures ( $F(1,7) = 0.0089$ ,  $p = 0.81$ ; see section 2.2 for description of deafening procedures). Comparisons were therefore performed using mass-univariate approach to compare hearing with deafened animals pooled from both deafening procedures (see section 2.8). Table 2 shows the results of a second repeated measures MANOVA test for significant main effects and interactions between three factors: 1) hearing vs deaf (all deafened animals), 2) male vs female, 3) age at scanning < 1 y vs age at scanning > 1 y. There were no significant (all  $p > 0.05$ ) main effects or interactions between any of the three factors.

### Spatial group independent component analysis

Resting-state fMRI data from both hearing and deaf cats were decomposed into 20 independent spatial components using group ICA. Fig. 4 shows all 20 thresholded networks (A-T) identified by brain regions included within the spatial networks. Back-reconstruction of spatial networks to individual subjects shows strong similarity between the hearing and deaf groups (Supplementary Fig. 2). The spatial extents of these networks were not significantly different between hearing and deaf cats (minimum between-group Pearson's  $r(18) = 0.62$ ,  $p < 0.001$ ).

Independent spatial networks were classified per the anatomical extents of their activation areas (see methods section 2.6, Fig. 4 and Supplementary Fig. 1): visual (10 networks; blue), auditory (3 networks; orange), somatosensory (1 network; green), cingulate/insular (3 networks; purple), and non-cortical (3 networks; gray). Networks were predominantly symmetric across hemispheres apart from two visual networks, O and P, which primarily encompassed the left or right suprasylvian sulci, respectively (Figs. 3 and 4).

### Non-cortical networks

Fig. 3 shows three bilateral networks primarily included caudate nucleus (A), periaqueductal gray (PAG)/inferior colliculus (IC; Network B), or the cerebellum (C). Network A was largely restricted to the caudate nucleus. Network B primarily encompassed PAG, but also included approximately one-third of the IC. Network C was restricted to the cerebellum.

### Auditory networks

Auditory related components included three bilaterally, nearly symmetric networks: dorsoposterior (D), ventral (E), and anterior (F) networks (Fig. 3). The dorsoposterior auditory network (D) encompasses all of PAF which is involved in spatial localization (“where”) behavior (Malhotra et al., 2004; Malhotra and Lomber, 2007) and pitch processing in the cat (Butler et al., 2015). This network also includes the majority of primary auditory cortex (A1), dorsal zone of auditory cortex (DZ), and the posterior auditory belt regions which have non-tonotopic auditory as well as extrastriate visual inputs (Bowman and Olson, 1988). The ventral auditory network (E) primarily encompassed higher-order auditory brain regions including bilateral temporal (TE) as well as posterior aspects of auditory insular (IN) cortex. The anterior auditory network (F) included bilateral IN and regions of the anterior ectosylvian sulcus, such as the field of the anterior ectosylvian sulcus (FAES) which is involved in

**Table 1**

Brain region abbreviations.

Anatomical regions from a functional atlas of the cat brain (Stolzberg et al., 2017).

Auditory	A1	Primary Auditory Cortex
	A2	Second Auditory Cortex
	AAF	Anterior Auditory Field
	dPE	Posterior Ectosylvian Auditory Cortex, dorsal division
	DZ	Dorsal Zone of Auditory Cortex
	pPE	Posterior Ectosylvian Gyrus, posterior division
	FAES	Field of the Anterior Ectosylvian Sulcus
	IN	Auditory Insular Cortex
	iPE	Posterior Ectosylvian Auditory Cortex, intermediate division
	PAF	Posterior Auditory Field
	TE	Temporal Cortex
	VAF	Ventral Auditory Field
	vPAF	Posterior Auditory Field, ventral division
	vPE	Posterior Ectosylvian Auditory Cortex, ventral division
	Somatosensory	1
2		Area 2, Primary Somatosensory Cortex
3a		Area 3a Primary Somatosensory Cortex
3b		Area 3b Primary Somatosensory Cortex
5al		Area 5a, lateral division
5am		Area 5a, medial division
5bl		Area 5b, lateral division
5bm		Area 5b, medial division
5m		Area 5, medial division
S2		Second Somatosensory Cortex
S2m		Second Somatosensory Cortex, medial division
S3		Third Somatosensory Cortex
S4		Fourth Somatosensory Cortex
S5		Fifth Somatosensory Cortex
Visual		17
	18	Area 18
	19	Area 19
	20a	Area 20a
	20b	Area 20b
	21a	Area 21a
	21b	Area 21b
	7a	Area 7, anterior division
	7m	Area 7, medial division
	7p	Area 7, posterior division
	AEV	Anterior Ectosylvian Visual Area
	ALLS	Anterolateral Lateral Suprasylvian area
	AMLS	Anteromedial Lateral Suprasylvian area
	CVA	Cingulate Visual Area
	DLS	Dorsolateral Suprasylvian Visual Area
PLLS	Posterolateral Lateral Suprasylvian area	
PMLS	Posteromedial Lateral Suprasylvian area	
PS	Posterior Suprasylvian Visual Area	
SVA	Splenic Visual Area	
VLS	Ventrolateral Suprasylvian Area	
Motor	4δ	Area Praecentralis Macrogyramidalis
	4fu	Area Praecentralis in fundo
	4γ	Area Praecentralis
Frontal	4sfu	Area Praecentralis supra fundo
	6aα	Area Frontalis Agranularis Medio-pyramidalis
	6aβ	Area Frontalis Agranularis Macro-pyramidalis
	6aγ	Area 6, lateral division
Pre-frontal	6iffu	Area 6, infra fundum
	PFdl	Prefrontal Cortex, dorsolateral division
	PFdm	Prefrontal Cortex, dorsomedial division
Insular	PFv	Prefrontal Cortex, ventral division
	36	Perirhinal Cortex
	Ald	Agranular Insular Area, dorsal division
Limbic	AIV	Agranular Insular Area, ventral division
	DI	Dysgranular Insular Area
	GI	Granular Insular Area
	CgA	Anterior Cingulate Area
Misc.	CgP	Posterior Cingulate Area
	PL	Prelimbic Area
	G	Primary Gustatory Area
	MZ	Multisensory Zone
Non-cortical	Pp	Prepyriform Cortex
	RS	Retrosplenial Area
	Hipp	Hippocampus
	LGN	Lateral Geniculate Nucleus
	MGB	Medial Geniculate Body

(continued on next page)

**Table 1** (continued)

CN	Caudate Nucleus
PAG	Periaqueductal Gray
Cbm	Cerebellum

**Table 2**

Statistical comparison of independent variables.

Results of three-way MANOVA for the factors of age (<1 y vs. > 1 y), Hearing Status (hearing vs. deaf), and sex (male vs. female). None of the main effects or interactions were found to be significant ( $\alpha = 0.05$ ).

Factor	DF	DF error	F-stat	p-value
Sex	1	12	1.7186	0.2144
HearingStatus	1	12	0.2793	0.6068
Age	1	12	3.3942	0.0903
Sex x Age	1	12	0.0514	0.8244
Hearing Status x Sex	1	12	0.7333	0.4086
Hearing Status x Age	1	12	0.0030	0.9574
Hearing Status x Age x Sex	1	12	0.1167	0.7385

orienting to acoustic stimuli of the contralateral hemifield in hearing cats, but switches to orienting towards contralateral visual stimuli in early deafened cats (Meredith et al., 2011).

### Visual networks

A large portion of cat cerebral cortex is dedicated to processing the visual world. Half of the networks identified with ICA presided predominantly in striate or extrastriate visual cortex (see Figs. 3 and 4, and Supplementary Fig. 1). Visual networks included the superior colliculus (SC; Network G), dorsoposterior (H), retrosplenial (I), posteromedial (J), anteromedial (K), posterolateral (L), anterolateral (M), and medial (N) visual cortical networks, and the right suprasylvian sulcus (O), and left suprasylvian sulcus (P).

One visual network, G, included the entire SC and was the only subcortical visual network identified. This network also included a portion of PAG, a nearby brainstem structure. Network H included approximately half of the dorsoposterior striate visual areas 17 and 18. Much of retrosplenial (RS) cortex was represented in network I, which also included nearby portions of the SC and hippocampus (Hipp) (Fig. 3).

The posteromedial network (J) was restricted to bilateral medial visual cortex, including portions of cingulate (CVA) and splenial visual areas (SVA), as well as retinotopic area 20b. Fig. 3 shows that the anteromedial network (K) also included anterior portions of bilateral SVA and medial visual area 7 m. Visual belt areas of the posterior suprasylvian gyrus (bilateral 21b) and sulcus (bilateral ventral and dorsal lateral suprasylvian areas, VLS and DLS respectively) were included in the posterolateral network (L). Area 7p was largely represented in the anterolateral network (M). Area 7p receives projections from areas of the lateral sulcus (AMLS, ALLS, and PLLS; Olson and Lawler, 1987) which were also partially included in the anterolateral network. Although partially represented in other networks, the SVA and CVA were primarily represented in the medial visual network (N). Networks O and P were the only lateralized networks identified with ICA and included the right and left suprasylvian sulci, respectively. These regions have been demonstrated to be involved in visual motion and spatial behavior (Lomber et al., 1996, 1994; Lomber and Payne, 2004).

### Somatosensory networks

One network, Q, represented somatosensory brain regions. This network included somatosensory regions located along the anterior ectosylvian gyrus: S2, S2m, S3, S4, and S5. Also included in this network were multisensory regions of the anterior bank of the suprasylvian sulcus: anterior ectosylvian visual area (AEV), multisensory zone (MZ), and portions of FAES (Fig. 3).

### Cingulate/insular networks

These networks included anterior insular (R), posterior cingulate (S),

and the anterior cingulate (T) brain regions. Dorsal (AId) and ventral (AIV) aspects of bilateral agranular insular cortex were included in network R. To a lesser extent, portions of granular (GI) and dysgranular (DI) insular cortex, as well as prepyriform cortex (Pp), were also present in this network (Fig. 3).

Network S included most of posterior cingulate cortex (CGp), a region involved in the default mode network (DMN) in several species (Hutchison et al., 2013, 2010; Kyathanahally et al., 2015; Lu et al., 2012; Zhou et al., 2016). Motor and premotor regions were also included in this network. The anterior cingulate (CGa), another region involved in DMN (Popa et al., 2009; Raichle et al., 2001) was entirely circumscribed by network T. This network also included large portions of motor (4sfu, 4y, 4δ, 6iffu, 6aα, 6aβ), and prelimbic cortex (PL) (Fig. 3).

### Functional network connectivity

Twenty networks were back-reconstructed from the group ICA, which included all hearing and deaf subject data, to individual subjects permitting group comparisons (see section 2.5). The amplitude ( $\rho$ ) and lag ( $\delta$ ) to the peak correlation were computed comparing all network time courses for each subject.

### Effects of deafness on amplitude of peak correlation – $\rho$

All between-group differences (deaf - hearing) in  $\rho$  are presented in Fig. 5A. In total, 190 comparisons were made between networks. Of these comparisons,  $\rho$  was found to be significantly different between hearing and deaf cats for 10 network comparisons ( $p_{FDR} < 0.05$ ; data in Table 3). A circular connectivity plot (Fig. 5B) shows significant between-group differences.

Between-group differences could reflect networks that are significantly correlated in both hearing and deaf animals, but which differ in the strength of that correlation. Alternatively, networks may be correlated in one group, but not correlated in the other group. Fig. 5C probes these relationships by plotting the distributions of hearing and deaf data separately for each significant between-group difference. Statistics for significant between-group differences are presented in Table 3. Within-group internetwork correlations were also evaluated for significance with a more restrictive criterion ( $p_{FDR} < 0.01$ ). All within-group correlations are presented in Fig. 6.

Of the ten network correlations that differed in amplitude between hearing and deaf animals, six involved auditory networks ( $p_{FDR} < 0.05$ ; Fig. 5C). Five of these six significant differences involved the dorsoposterior auditory network (D). The dorsoposterior auditory network (D) showed a larger amplitude correlation with non-auditory networks in deaf than in normal hearing in three of these internetwork differences. The correlation between the dorsoposterior auditory network (D) and the cerebellar network (C) was significantly positively correlated in deaf, but was not correlated in hearing cats. A significant, but small anticorrelation was measured for hearing cats between dorsoposterior auditory network (D) and the caudate nucleus network (A). In deaf cats, the mean correlation between these networks was positive but was not significant due to the large subject variance in  $\rho$ . The correlation between dorsoposterior auditory network (D) and the superior colliculus network (G) showed the opposite pattern. There was a significant positive correlation in deaf cats between dorsoposterior auditory network (D) and the superior colliculus network (G), whereas there was no significant correlation for the hearing cats.

The remaining three significant changes in auditory network connectivity involved a decrease in correlation amplitude in the deaf, relative to normal hearing animals (Fig. 5C). A significant positive correlation was measured between dorsoposterior auditory network (D) and the anterior auditory network (F) in hearing, whereas deaf cats did not exhibit a significant correlation between these two auditory networks. The significant decrease between the dorsoposterior auditory network (D) and posteromedial visual network (J) in deaf compared with hearing was due to an increase in the anticorrelation between these networks in

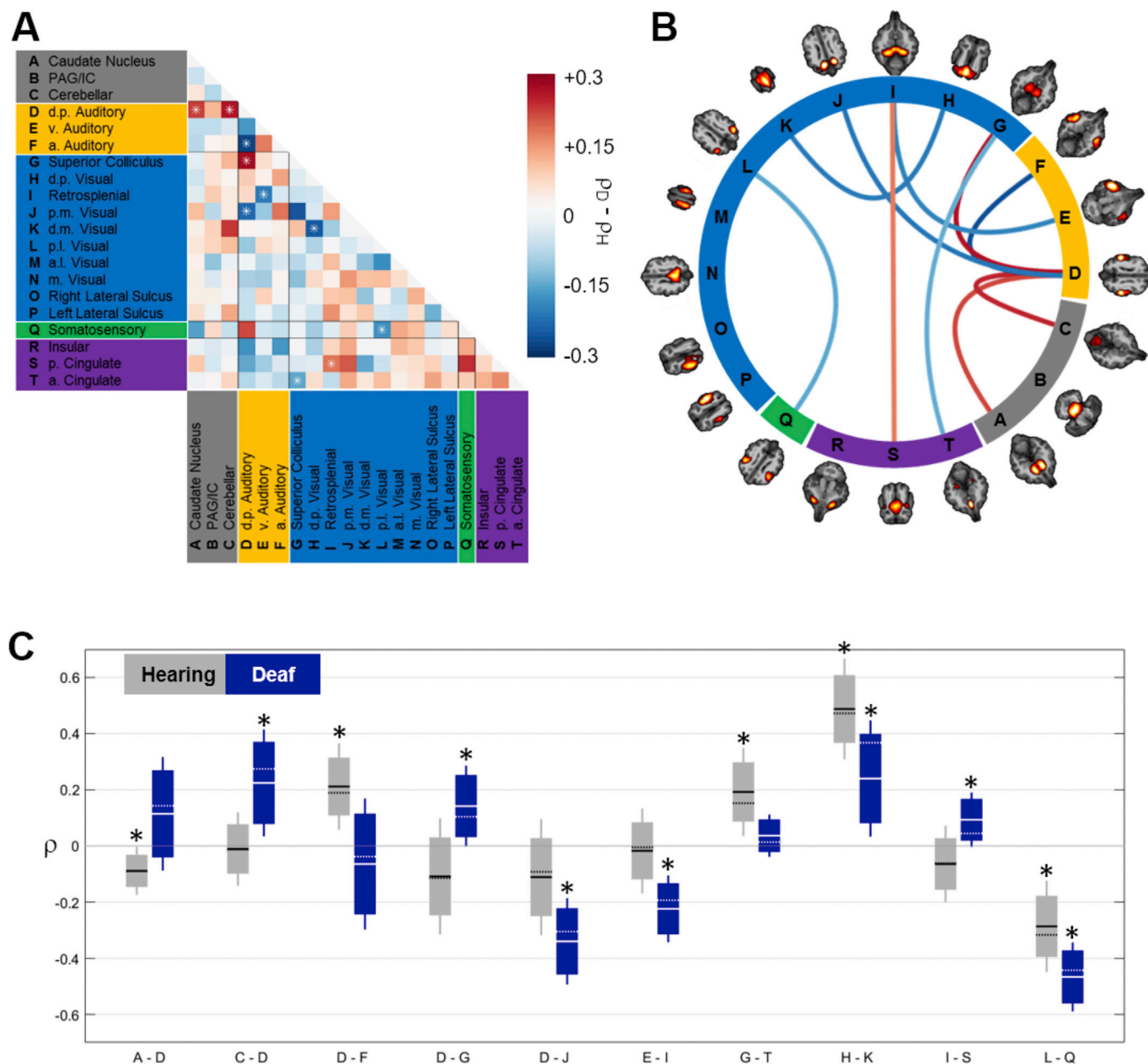


**Fig. 5. Between-Group Differences in Mean Functional Network Correlation.** A. Matrix shows differences in peak correlation,  $\rho$ , between groups ( $\rho_D - \rho_H$ ). Only one-half of the symmetric matrix is shown since only one absolute peak value was analyzed for each comparison. Asterisks overlying network comparisons on the heat map indicate significant between-group differences ( $P_{FDR} < 0.05$ ). B. Significant differences from panel A are shown on a circle plot between networks. Color of the lines connecting the networks is scaled to the color bar in panel A. Axial brain slices are oriented with brain anterior direction oriented outward. C. The same significant between-group correlations presented in panel B, but of the within-group distributions of  $\rho$ . Boxes indicate  $\pm 1$  standard deviation, vertical lines indicate 95% confidence interval, solid and dotted horizontal lines indicate sample mean and median, respectively. Within-group significance is indicated \* =  $P_{FDR} < 0.01$ . See Table 3 for statistics.

**Table 3**

Significant within-group and between-group differences in  $\rho$ .

Within-group values,  $\rho_D$  and  $\rho_H$ , are represented as mean  $\pm$  standard error of the mean. Between-group values,  $\rho_D - \rho_H$ , are represented as mean  $\pm$  1 standard deviation. Effect sizes are calculated as using Hedge's  $g$ . P-values are corrected for false-discovery rate (within-group  $\alpha_{FDR} = 0.01$ ; between-group  $\alpha_{FDR} = 0.05$ ). Degrees of freedom:  $\rho_D = 8$ ;  $\rho_H = 10$ ;  $\rho_D - \rho_H = 18$ . See section 2.8 for details on statistics.

Networks	$\rho_D$	$g_1$	$P_{FDR}$	$\rho_H$	$g_1$	$P_{FDR}$	$\rho_D - \rho_H$	$g$	$P_{FDR}$
A–D	+0.114 $\pm$ 0.067	0.566	0.060	−0.089 $\pm$ 0.028	−1.041	<0.001	+0.203 $\pm$ 0.069	1.307	0.019
C–D	+0.224 $\pm$ 0.063	1.181	<0.001	−0.011 $\pm$ 0.044	−0.082	0.406	+0.235 $\pm$ 0.070	1.409	0.015
D–F	−0.064 $\pm$ 0.078	−0.276	0.229	+0.212 $\pm$ 0.051	1.378	<0.001	−0.275 $\pm$ 0.086	−1.368	0.015
D–G	+0.142 $\pm$ 0.048	0.986	<0.001	−0.108 $\pm$ 0.069	−0.525	0.061	+0.250 $\pm$ 0.075	1.321	0.015
D–J	−0.340 $\pm$ 0.051	−2.214	<0.001	−0.111 $\pm$ 0.069	−0.537	0.059	−0.229 $\pm$ 0.077	−1.185	0.044
E–I	−0.224 $\pm$ 0.040	−1.886	<0.001	−0.017 $\pm$ 0.050	−0.115	0.374	−0.207 $\pm$ 0.057	−1.436	0.015
G–T	+0.036 $\pm$ 0.025	0.484	0.083	+0.192 $\pm$ 0.052	1.225	<0.001	−0.156 $\pm$ 0.050	−1.172	0.028
H–K	+0.240 $\pm$ 0.069	1.161	0.002	+0.488 $\pm$ 0.060	2.718	<0.001	−0.247 $\pm$ 0.083	−1.234	0.030
I–S	+0.093 $\pm$ 0.032	0.962	0.002	−0.064 $\pm$ 0.046	−0.471	0.079	+0.157 $\pm$ 0.050	1.252	0.015
L–Q	−0.466 $\pm$ 0.041	−3.803	<0.001	−0.287 $\pm$ 0.054	−1.765	<0.001	−0.180 $\pm$ 0.061	−1.180	0.016

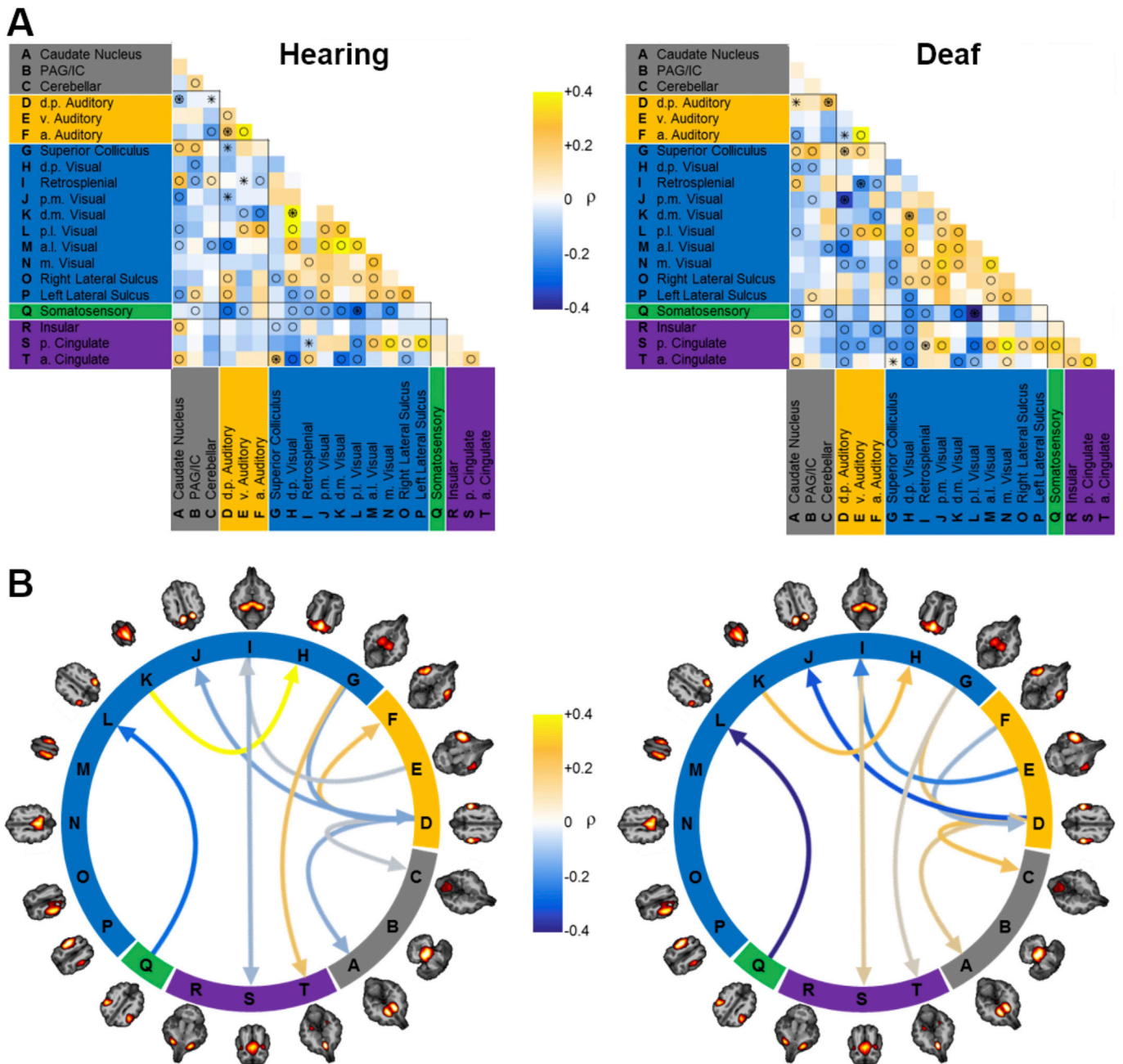


**Fig. 6. Within-Group Mean Functional Network Correlations.** A. The mean amplitude of the peak correlation,  $\rho$ , between each network is displayed as a colored map where yellow is a positive correlation and blue is an anti-correlation between network time courses. Asterisks and circles overlying network comparisons on the heat maps indicate significant between-group differences and within-group correlations, respectively (also see Fig. 5). B. The lines connecting network pairs indicate the within-group value of  $\rho$  as well as the mean direction of lag,  $\delta$  (Fig. 7); networks receiving the arrow lag the originating network. For example, in both plots, network L lags network Q.

both groups. The ventral auditory network (E) was significantly anti-correlated with the retrosplenial network (I) in deaf, but was not correlated in hearing cats.

A significant decrease in correlation was observed in deaf cats between the anterior cingulate network (T) and the superior colliculus network (G). These networks were positively correlated in hearing cats, but not significantly correlated in deaf cats. The dorsoposterior visual network (H) and the dorsomedial visual network (K) were significantly positively correlated in both hearing and deaf cats; however, deaf cats exhibited a significantly reduced correlation compared with hearing cats. The posterior cingulate network (S) was significantly positively correlated with the retrosplenial network (I) in deaf cats, whereas these networks were not correlated in hearing cats. Both hearing and deaf cats exhibited significant anticorrelations between the posterolateral visual

network (L) and the somatosensory network (Q); the anticorrelation between these networks was significantly greater (more anticorrelated) for deaf than hearing cats.

*Effects of deafness on lag to peak correlation –  $\delta$*

Within-group peak amplitude correlations,  $\rho$ , were significant ( $p_{FDR} < 0.01$ ) for 73 (38.4%) and 75 (39.5%) of the 190 network interactions for deaf and hearing cats, respectively (Fig. 6A). Of these correlation amplitudes, 45 (23.7%) were significant for both groups. The temporal lags (the delay to the peak correlation between networks;  $\delta$ ) between groups were compared for these 45 correlations. Temporal relationships between networks were not significantly different ( $p_{FDR} < 0.05$ ) when deaf and hearing groups were compared for any of the 45 network correlations evaluated. The internetwork lags,  $\delta$ , for all

correlations tested are presented in Fig. 7.

**Discussion**

Brain development in the absence of a sense leads to compensatory plasticity and, ultimately, behaviorally identifiable changes in the remaining sensory modalities. Early sensory loss may also result in a general loss of function in brain regions which normally process the lost modality. Here we report several significant differences in functional connectivity between brain networks in deaf and hearing cats. The primary findings are schematized in Fig. 8 (see Supplementary Fig. 3 for a more detailed summary). Taken together, the results indicate that both compensatory plasticity and a general loss of function likely coexist between various networks the deaf brain. The majority of group differences in FNC amplitude included regions involved in oculomotor and spatial localization functions.

*Early deafening and maturation of cat auditory pathway*

A kitten's ear canal is sealed at birth, opening around postnatal day 10 (P10), however ABRs can be detected as early as P2 in response to loud acoustic stimuli (90 dB SPL tones (Pujol and Marty, 1970); 130 dB peak SPL clicks (Walsh et al., 1986a)) if the ear canal is surgically opened. This early functional development reflects closely the altricial structural maturation of the cochlea which is mature by the second postnatal week (Pujol and Marty, 1970). The latencies of sound-evoked ABR waveforms decrease linearly with age (Walsh et al., 1986b) while the waveform amplitudes do not stabilize until approximately the third postnatal month (Walsh et al., 1986c). Tonotopy, a basic feature representing frequency selectivity in structures of the ascending lemniscal auditory pathway, is already approaching maturity in the inferior colliculus by the third postnatal week (Aitkin and Moore, 1975). The amplitude and latency of neural responses in cat A1 increase rapidly during the first postnatal month (Eggermont, 1996; Walsh et al., 1986c); however, representation of more temporally complex sound stimuli slowly approaches maturity until sometime during the third postnatal month (Eggermont, 1996, 1991).

In the present study, we used two methods to induce deafening in 9

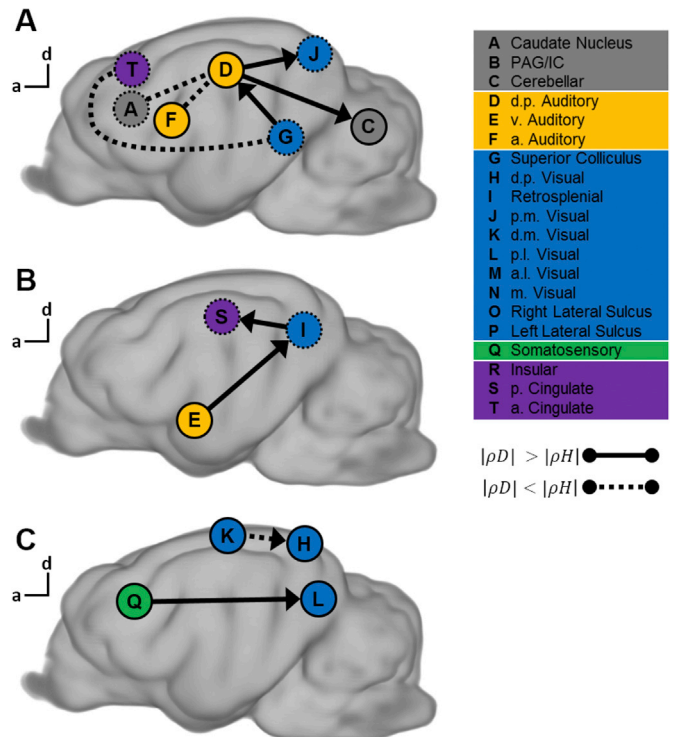


**Fig. 8. Summary of Significant Functional Connectivity Differences in Deaf Cats.** Significant between-group differences in functional network connectivity (FNC),  $\rho$ , are presented over the lateral view of the cat brain. Circles with letters indicate approximate locations of networks. Solid (dotted) lines indicate absolute value of  $\rho$  was greater (less) in deaf than hearing cats. Arrows indicate the direction of influence of one network on another where  $\rho$  was significant in deaf cats. The arrow points to the network that lags that of the originating network (see Fig. 7). ‘a’ and ‘d’ indicate anterior and dorsal directions, respectively. See Supplementary Fig. 3 for a more detailed schematic of these findings.

cats prior to the complete maturation of the cat's auditory system. Deafening within the first postnatal month has been shown to elicit significant restructuring of anatomical projections within and targeting

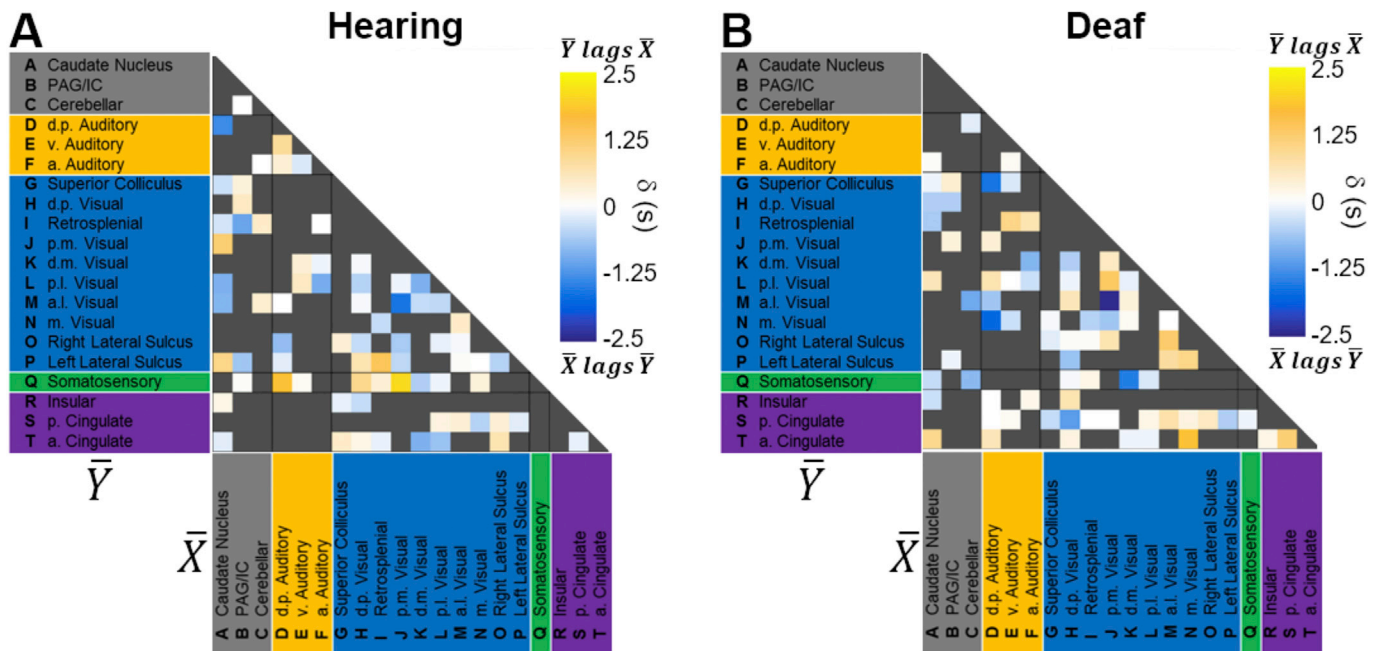


**Fig. 7. Within-Group Functional Network Connectivity Peak Lag ( $\delta$ ).** Mean lag,  $\delta$ , of significant internetwork correlations,  $\rho$ , are displayed for the hearing (A) and deaf (B) groups. Grayed-out comparisons are where the internetwork correlations did not reach significance (see Fig. 6). A positive  $\delta$  indicates that  $Y'$  lags  $X'$ , whereas a negative  $\delta$  indicates  $X'$  lags  $Y'$ .

auditory cortex of the cat (Butler et al., 2016a; Kok et al., 2014; Wong et al., 2015).

#### Effects of deafness on auditory internetwork correlations

When deaf and hearing cats were compared, changes in internetwork correlation predominantly involved the dorsoposterior auditory network (D), which includes A1, DZ, PAF, vPAF, and auditory belt regions of the posterior ectosylvian gyrus (Fig. 8A). Among other functions, these regions play a central role in the auditory “where” pathway (Lomber and Malhotra, 2008). In congenitally deaf cats, PAF has been shown to subserve improved localization of peripheral visual stimuli (Lomber et al., 2010).

A loss of correlation was observed in deaf cats between the dorsoposterior network (D) and the anterior auditory network (F) (Fig. 8A) in which FAES was largely represented (Fig. 4, Supplementary Fig. 1). Single-unit recordings in hearing cat FAES indicate that the preponderance of neurons are auditory, with approximately one-third of the population exhibiting audio-visual or audio-somatosensory sensitivity (Meredith et al., 2011). FAES is involved in acoustic orienting behavior in hearing cats (Malhotra et al., 2004; Malhotra and Lomber, 2007); however, FAES has been shown to switch modalities in the deaf brain to visual orientation (Meredith et al., 2011). The reduction in functional connectivity between the anterior and dorsoposterior auditory networks reported here may reflect a reduced influence of early auditory cortex on FAES despite a lack of changes in projections to FAES in deaf cats when compared to normal hearing animals (Meredith et al., 2016). A reduction in correlation between auditory structures parallels fMRI experiments in congenitally blind subjects. Liu et al. (2007) demonstrated a similar significant decrease in correlated resting-state blood-oxygen-level-dependent (BOLD) fluctuations within occipital cortices compared with sighted individuals.

In the current study, the dorsoposterior auditory and posteromedial visual networks (D & J) were shown to be more strongly anticorrelated in deaf than in normal hearing cats (Fig. 8A). The posteromedial visual network includes visual area 20b bilaterally, which contain spatially tuned neurons representing a large portion of central and peripheral field (Updyke, 1986). Anatomical tracer studies did not identify direct projections to PAF from area 20b in hearing or early deaf (Butler et al., 2016a) cats. We speculate that the change in functional connectivity between these two networks may be conferred by way of an intermediary brain region.

The cerebellar network (C) was found to be significantly correlated with the dorsoposterior auditory network (D) in deaf, but not hearing subjects (Fig. 8A). The cerebellum, a structure classically involved in motor function, has been demonstrated to be responsive to sound (Altman et al., 1976; Fadiga and Pupilli, 1964) as well as direct electrical stimulation of cat auditory cortex (Hampson, 1949). Altman et al. (1976) found that cerebellar neurons in the cat exhibited poor sound frequency selectivity, but were selective for sound movement direction and interaural time and intensity differences indicating a role for the cerebellum in sound localization. The cerebellum is also responsive to visual stimulation (Fadiga and Pupilli, 1964) and has overlapping visual and auditory representations on the cat cerebellar vermis (Fuchs and Kornhuber, 1969; Snider and Stowell, 1944). Furthermore, the cerebellum is known to be involved in oculomotor control including reflexive, voluntary, and smooth pursuit saccades (Colnaghi et al., 2010; Fuchs and Kornhuber, 1969; Kleine et al., 2003; Ron and Robinson, 1972). The caudal fastigial nucleus (cFN), a small cerebellar structure that receives projections from Purkinje cells of the vermis, plays a key role in adaptive control of gaze accuracy (Goffart, 2004; Kleine et al., 2003; Krauzlis et al., 2017). Temporary inactivation of the cFN in monkeys resulted in reduced accuracy in landing on visual targets primarily in the horizontal, and very little in the vertical, saccade components (Goffart, 2004).

The posterior auditory field, PAF, which is included in the dorsoposterior auditory network (D; Fig. 8A), has been demonstrated to be

involved in supranormal sound localization ability in congenitally deaf cats (Lomber et al., 2010). It is plausible that in deaf animals, brain regions typically involved in sound localization are more strongly coupled to the cerebellum resulting in improved performance on visual tasks. Projections to the dorsolateral pontine nucleus, which itself provides the majority of projections to the cerebellum, have been identified from both auditory cortex (Knowlton et al., 1993) and inferior colliculus (Huffman and Henson, 1990). Furthermore, these projections are reciprocated, at least via polysynaptic connectivity, since electrical stimulation of the auditory responsive cerebellar vermis results in activation of inferior colliculus, medial geniculate body, and a large proportion of auditory cortex (Snider and York, 1966). To our knowledge no studies have directly investigated the functional role of the cerebellum in deaf subjects. The functional connectivity observed in the current study in deaf, but not hearing, cats indicates that the cerebellum may be a novel region of research in deafness and possibly other developmental sensory deficits.

Similar to the enhanced auditory-cerebellar functional connectivity, the superior colliculus network (G) was also significantly correlated with the dorsoposterior auditory network (D) in deaf, but not hearing animals (Fig. 8A). The anatomical and functional nature of auditory cortical projections to the superior colliculus (SC) are well described. SC receives direct corticofugal projections primarily from visual cortex, however, a subset of projections is received from auditory cortex. Most auditory cortical projections to SC originate in FAES (Butler et al., 2016b; Zingg et al., 2017), represented in the anterior auditory network (F). The second largest projection from auditory cortex to SC originates from PAF (Butler et al., 2016b) which had the highest median z-score in the dorsoposterior auditory network (D; see Fig. 4). The neighboring posterior medial and lateral portions of the suprasylvian sulcus also have strong projections to SC (Butler et al., 2016b), however these areas were not well represented in the dorsoposterior auditory network (Fig. 4, Supplementary Fig. 1).

The caudate nucleus network (A) was not correlated with the dorsoposterior auditory network (D) in deaf (Fig. 8A), but was significantly anticorrelated in hearing cats. The caudate nucleus (CN), part of the dorsal striatum, is involved in movement control and receives broad cortical inputs. Projections to the CN from auditory cortex are present in cat (Rosell and Giménez-Amaya, 1999) whereas the medial geniculate body is devoid of projections (Royce, 1978). Although we know of no studies investigating anatomical connectivity in deaf cat CN, the absence of significant functional connectivity observed in the current study may reflect the pruning of projections from auditory cortex to CN during development in the deaf. CN plays a central role in human language production (Abutalebi and Green, 2016; Crinion et al., 2006) and gray matter volume of CN has been found to be significantly affected by sign language experience in the deaf (Olulade et al., 2014). The decoupling of CN and dorsoposterior auditory cortex observed in deaf cats may reflect developmental neuroplasticity in the absence of auditory input.

The ventral auditory network (E), which includes auditory insular (IN) and temporal (TE) cortex, was found to be significantly anticorrelated with the retrosplenial network (I) in deaf (Fig. 8B), but not significantly correlated in hearing cats. IN is a higher-level auditory region of the ventral ectosylvian gyrus which is also responsive to visual and auditory-visual stimuli (Diego and Jolla, 1977; Loe and Benevento, 1969). Visual modulation of IN is likely a result of its monosynaptic reciprocal connections with dorsal posterior suprasylvian gyrus (Lee and Winer, 2008) which is responsive to auditory and visual stimulation. Although the functional role of cat TE is not entirely clear, this region is heavily interconnected with multisensory ventral posterior suprasylvian gyrus, IN, and second auditory cortex (Lee and Winer, 2008). Given the strong anatomical integration between TE and multisensory areas, we suspect TE to be involved in higher-order object processing. Indeed, human and non-human primates inferotemporal cortex is involved in visual object and face discrimination (Afraz et al., 2006; Kriegeskorte et al., 2008). Retrosplenial (RS) cortex, representing the posterior aspect

of CGp, is not well understood, but is thought to be involved in visuo-spatial memory processing (Vann et al., 2009). The significant anti-correlation between the ventral auditory network (E) and retrosplenial network (I) in deaf cats may indicate a novel functional coupling between these two brain regions. If cat IN and/or TE are indeed involved in higher-order multisensory object processing in hearing animals, then increased coordination with RS may indicate a more significant role of ventral suprasylvian gyrus in visual object processing in deafness.

#### *Effects of deafness on non-auditory internetwork correlations*

In hearing cats, the superior colliculus network (G) exhibited significant functional connectivity with the anterior cingulate network (T); however, this interregional correlation was not significant in deaf cats (Fig. 8A). Although the anterior cingulate (CGa) was the dominant area represented in network T, all subdivisions of areas 4 and 6 (except for 6a) as well as prefrontal (PL) cortex were also represented (Fig. 4, Supplementary Fig. 1). There exists no evidence of direct projections between SC and CGa in hearing cats (Butler et al., 2016b; Musil and Olson, 1988); however, neurons of CGa, PL, and pericruciate cortex (including areas 4 and 6) make reciprocal projections with periaqueductal gray (PAG; also included in network G, Fig. 4 and Supplementary Fig. 1) (Bandler et al., 1985; Matsuyama and Drew, 1997). Interestingly, electrical stimulation of either CGa or PAG results in evoked vocalizations in cats and monkeys (Devinsky et al., 1995). Furthermore, severing the pathway linking CGa with PAG in squirrel monkeys results in the abolishment of CGa-evoked vocalizations since PAG projects directly to nucleus ambiguus, the area responsible for laryngeal control (Devinsky et al., 1995; Jürgens and Pratt, 1979). Although mature deaf cats vocalize (Shiple et al., 1988), they presumably have very limited experience with vocalizations during the short period prior to deafening. This lack of (or reduced) experience with vocalizations may lead to improper formation of vocalization circuits as reflected in the lack of significant functional connectivity between these areas. Somewhat discordant with this hypothesis, the anterior cingulate network (T) was not found to be significantly different in correlation with PAG/IC network (B) between hearing and deaf cats. Networks B and G included the ventral and dorsal aspects of PAG, respectively (see Fig. 3), and this spatial segregation may be important in vocal function (cf. Jürgens and Pratt, 1979).

Two of the 10 between-group differences in  $\rho$  were found to be significantly correlated in both groups. The dorsoposterior visual network (H) and the dorsomedial visual network (K) were significantly correlated in both groups (Fig. 8C), but significantly less so within the deaf compared with the hearing cats. The dorsoposterior network (H) included early visual areas 17 and 18, whereas the dorsomedial visual network (K) primarily included area 7 m and the splenial visual area (SVA). The SVA is a small visual region neighboring area 17 on the medial aspect of the cortex. Interestingly, neurons in SVA are predominantly sensitive to horizontal orientations localized to the extreme visual peripheral field (Kalia and Whitteridge, 1973). The decrease in correlation between SVA and earlier visual areas at rest may indicate that SVA plays a more distinct role in processing peripheral visual stimuli in deaf cats.

The opposite change in correlation was observed between hearing and deaf cats for the relationship between somatosensory (Q) and posterolateral visual (L) networks (Fig. 8C). These networks were significantly more anticorrelated in the deaf than in the hearing group. The enhanced anticorrelation between the somatosensory and visual networks at rest in deaf cats may reflect neuroplastic changes involved in mediating somato-visual interactions. In a human behavioral/fMRI study, Karns et al. (2012) found that congenitally deaf, but not hearing, subjects were susceptible to a visual-somatosensory double-flash illusion. That study further found a significant correlation between activation of auditory cortex and the perception of the illusion. The visual-somatosensory double-flash illusion has yet to be tested in

deaf animals.

#### *Effects of deafness on default mode network*

The default mode network (DMN) is characterized by the large-scale functional correlation of several brain regions while at rest (Raichle et al., 2001; Smith et al., 2009). Every mammalian species investigated to date has been observed to have a DMN while awake (Belcher et al., 2013; Hutchison et al., 2013, 2010; Kyathanahally et al., 2015; Lu et al., 2012; Upadhyay et al., 2011; Zhou et al., 2016) or lightly anesthetized (Hutchison et al., 2013, 2010; Vincent et al., 2007). Brain regions involved in DMN include CGa, CGp, RS, medial prefrontal cortices, and insular areas (Greicius et al., 2009).

While the current study is the first report of resting-state functional networks in the cat using fMRI, Popa et al. (2009) investigated the electrophysiological correlates of the DMN in chronically implanted cats. That study observed enhanced correlation between CGa and CGp while at rest. In agreement, the current fMRI study also found that cat posterior cingulate (S) and anterior cingulate (T) brain regions were significantly correlated in both hearing and deaf cats (Fig. 6).

Hearing and deaf cats exhibited a similar pattern of functional connectivity between posterior and anterior cingulate networks and all other networks (Fig. 6A) apart from the posterior cingulate and retrosplenial networks. The posterior cingulate network (S) was significantly correlated with the retrosplenial network (I) in deaf, but not hearing cats. RS represents the posterior subregion of CGp and these two regions are heavily interconnected in cats (Musil and Olson, 1993). The lack of correlation between RS and CGp in hearing cats differs from the findings in awake cats by Popa et al. (2009).

#### *Experimental considerations*

Scanner noise is one possible confound when studying resting-state networks (Gaab et al., 2008). Despite measures to significantly attenuate scanner noise from the cats using dense foam padding and insert foam earbuds, it is plausible that some of the differences in functional network interactions are due to acoustic activation of the hearing cat auditory system. Several of the significant differences in FNC between hearing and deaf cats identified here involved audio-visual networks and four differences in FNC did not involve auditory regions (Fig. 8). These results identify significant neuroplastic developmental differences in auditory as well as non-auditory networks that warrant further investigation with more invasive techniques.

#### **Conclusion**

The gains in FNC observed here support a role for neurodevelopmental changes in compensatory plasticity following early onset deafness. These gains, observed as increased between-network correlations and anticorrelations, may reflect the altered intrinsic functional and/or anatomical connectivity subserving enhanced processing in non-deprived modalities. Decreases in correlations between networks indicate a loss of function in brain regions deprived of normal sensory inputs during critical stages during development. Functional network connectivity analysis in hearing and deaf cats revealed that both gain and loss of function coexist within the same brain following early sensory deprivation. Furthermore, these results reveal novel targets for more detailed anatomical, electrophysiological, and behavioral exploration into the neuroplastic changes associated with early onset deafness.

#### **Funding**

Funding for this project was provided by the Natural Sciences and Engineering Research Council of Canada, the Canadian Institutes of Health Research, the Canada Foundation for Innovation, and the Centre for Functional and Metabolic Mapping.

## Conflict of interest

None.

## Acknowledgments

The authors would like to thank Pam Nixon, RVT for providing animal care, Dr. Joseph Gati, Trevor Szekeres, and Dr. Kyle Gilbert for help with fMRI data acquisition and equipment, and Dr. Melissa L. Caras for helpful comments on the manuscript.

## Appendix A. Supplementary data

Supplementary data related to this article can be found at <https://doi.org/10.1016/j.neuroimage.2017.10.002>.

## References

- Abutalebi, J., Green, D.W., 2016. Neuroimaging of language control in bilinguals: neural adaptation and reserve. *Biling. Lang. Cogn.* 19, 1–10. <https://doi.org/10.1017/S1366728916000225>.
- Afraz, S.R., Kiani, R., Esteky, H., 2006. Microstimulation of inferotemporal cortex influences face categorization. *Nature* 442, 692–695. <https://doi.org/10.1038/nature05153>.
- Aitkin, L.M., Moore, D.R., 1975. Inferior colliculus II. Development of tuning characteristics and tonotopic organization in central nucleus of the neonatal cat. *J. Neurophysiol.* 38, 1208–1216.
- Altman, J.A., Bechterev, N.N., Radionova, E.A., Shmigidina, G.N., Syka, J., 1976. Electrical responses of the auditory area of the cerebellar cortex to acoustic stimulation. *Exp. Brain Res.* 26, 285–298. <https://doi.org/10.1007/BF00234933>.
- Ashburner, J., 2007. A fast diffeomorphic image registration algorithm. *NeuroImage* 38, 95–113. <https://doi.org/10.1016/j.neuroimage.2007.07.007>.
- Bandler, R., McCulloch, T., Dreher, B., 1985. Afferents to a midbrain periaqueductal grey region involved in the “defence reaction” in the cat as revealed by horseradish peroxidase. I. The telencephalon. *Brain Res.* 330, 109–119. [https://doi.org/10.1016/0006-8993\(85\)90011-3](https://doi.org/10.1016/0006-8993(85)90011-3).
- Barone, P., Lacassagne, L., Kral, A., 2013. Reorganization of the connectivity of cortical field DZ in congenitally deaf cat. *PLoS One* 8 (4), e60093.
- Bavelier, D., Brozinsky, C., Tomann, A., Mitchell, T., Neville, H., Liu, G., 2001. Impact of early deafness and early exposure to sign language on the cerebral organization for motion processing. *J. Neurosci.* 21, 8931–8942. <https://doi.org/10.1523/JNEUROSCI.2122-01.2001>.
- Bavelier, D., Neville, H.J., 2002. Cross-modal plasticity: where and how? *Nat. Rev. Neurosci.* 3, 443–452. <https://doi.org/10.1038/nrn848>.
- Behzadi, Y., Restom, K., Liu, J., Liu, T.T., 2007. A component based noise correction method (CompCor) for BOLD and perfusion based fMRI. *NeuroImage* 37, 90–101. <https://doi.org/10.1016/j.neuroimage.2007.04.042>.
- Belcher, A.M., Yen, C.C., Stepp, H., Gu, H., Lu, H., Yang, Y., Silva, A.C., Stein, E.A., 2013. Large-scale brain networks in the awake, truly resting marmoset monkey. *J. Neurosci.* 33, 16796–16804. <https://doi.org/10.1523/JNEUROSCI.3146-13.2013>.
- Berman, A.L., Jones, E.G., 1982. The Thalamus and Basal Telencephalon of the Cat. A Cytoarchitectonic Atlas with Stereotaxic Coordinates. University of Wisconsin Press, Madison.
- Bola, Ł., Zimmermann, M., Mostowski, P., Jednoróg, K., Marchewka, A., Rutkowski, P., Szewd, M., 2017. Task-specific Reorganization of the Auditory Cortex in Deaf Humans. *PNAS*, 201609000.
- Bowman, E.M., Olson, C.R., 1988. Visual and auditory association areas of the cat's posterior ectosylvian gyrus: cortical afferents. *J. Comp. Neurol.* 272, 30–42. <https://doi.org/10.1002/cne.902720104>.
- Brown, T.A., Joannisse, M.F., Gati, J.S., Hughes, S.M., Nixon, P.L., Menon, R.S., Lomber, S.G., 2013. Characterization of the blood-oxygen level-dependent (BOLD) response in cat auditory cortex using high-field fMRI. *NeuroImage* 64, 458–465. <https://doi.org/10.1016/j.neuroimage.2012.09.034>.
- Butler, B.E., Chabot, N., Lomber, S.G., 2016a. Quantifying and comparing the pattern of thalamic and cortical projections to the posterior auditory field in hearing and deaf cats. *J. Comp. Neurol.* 524, 3042–3063. <https://doi.org/10.1002/cne.24005>.
- Butler, B.E., Chabot, N., Lomber, S.G., 2016b. A quantitative comparison of the hemispheric, areal, and laminar origins of sensory and motor cortical projections to the superior colliculus of the cat. *J. Comp. Neurol.* 524, 2623–2642. <https://doi.org/10.1002/cne.23980>.
- Butler, B.E., Hall, A.J., Lomber, S.G., 2015. High-field functional imaging of pitch processing in auditory cortex of the cat. *PLoS One* 10, 1–13. <https://doi.org/10.1371/journal.pone.0134362>.
- Chabot, N., Butler, B.E., Lomber, S.G., 2015. Differential modification of cortical and thalamic projections to cat primary auditory cortex following early- and late-onset deafness. *J. Comp. Neurol.* 523 (15), 2297–2320.
- Calhoun, V.D., Adali, T., Pearlson, G.D., Pekar, J.J., 2001. A method for making group inferences from functional MRI data using independent component analysis. *Hum. Brain Mapp.* 14, 140–151. <https://doi.org/10.1002/hbm.1048>.
- Chai, X.J., Castañán, A.N., Öngür, D., Whitfield-Gabrieli, S., 2012. Anticorrelations in resting state networks without global signal regression. *NeuroImage* 59, 1420–1428. <https://doi.org/10.1016/j.neuroimage.2011.08.048>.
- Colnaghi, S., Ramat, S., D'Angelo, E., Versino, M., 2010. Transcranial magnetic stimulation over the cerebellum and eye movements: state of the art. *Funct. Neurol.* 25, 165–171. <https://doi.org/10.1017/S1127761>.
- Crinion, J., Turner, R., Grogan, A., Hanakawa, T., Noppeney, U., Devlin, J.T., Aso, T., Urayama, S., Fukuyama, H., Stockton, K., Usui, K., Green, D.W., Price, C.J., 2006. Language control in the bilingual brain. *Science* 80 (312), 1537–1540. <https://doi.org/10.1126/science.1127761>.
- Devinsky, O., Morrell, M.J., Vogt, B.A., 1995. Contributions of anterior cingulate cortex to behaviour. *Brain* 118 (Pt 1), 279–306. <https://doi.org/10.1093/brain/118.1.279>.
- Diego, S., Jolla, L., 1977. Auditory-visual interaction in cat orbital-insular cortex. *Neurosci. Lett.* 6, 143–149.
- Eggermont, J., 1996. Differential maturation rates for response parameters in cat primary auditory cortex. *Audit. Neurosci.* 2, 309–327.
- Eggermont, J.J., 1991. Maturation aspects of periodicity coding in cat primary auditory cortex. *Hear. Res.* 57, 45–56.
- Fadiga, E., Pupilli, G.C., 1964. Teleceptive components of the cerebellar function. *Physiol. Rev.* 44, 432–486.
- Fuchs, A.F., Kornhuber, H.H., 1969. Extraocular muscle afferents to the cerebellum of the cat. *J. Physiol.* 200, 713–722. <https://doi.org/10.1113/jphysiol.1969.sp008718>.
- Gaab, N., Gabrieli, J.D., Glover, G.H., 2008. Resting in peace or noise: scanner background noise suppresses default-mode network. *Hum. Brain Mapp.* 29 (7), 858–867. <https://doi.org/10.3389/fnhum.2010.00218>.
- Gilbert, K.M., Gati, J.S., Barker, K., Everling, S., Menon, R.S., 2016. Optimized parallel transmit and receive radiofrequency coil for ultrahigh-field MRI of monkeys. *NeuroImage* 125, 153–161. <https://doi.org/10.1016/j.neuroimage.2015.10.048>.
- Goffart, L., 2004. Deficits in saccades and fixation during muscimol inactivation of the caudal fastigial nucleus in the rhesus monkey. *J. Neurophysiol.* 92, 3351–3367. <https://doi.org/10.1152/jn.01199.2003>.
- Greicius, M.D., Supekar, K., Menon, V., Dougherty, R.F., 2009. Resting-state functional connectivity reflects structural connectivity in the default mode network. *Cereb. Cortex* 19, 72–78. <https://doi.org/10.1093/cercor/bhn059>.
- Hall, A.J., Brown, T.A., Grahn, J. a., Gati, J.S., Nixon, P.L., Hughes, S.M., Menon, R.S., Lomber, S.G., 2014. There's more than one way to scan a cat: imaging cat auditory cortex with high-field fMRI using continuous or sparse sampling. *J. Neurosci. Methods* 224, 96–106. <https://doi.org/10.1016/j.jneumeth.2013.12.012>.
- Hampson, J.L., 1949. Relationships between cat cerebral and cerebellar cortices. *J. Neurophysiol.* 12, 37–50.
- Hedges, L.V., 1981. Distribution theory for Glass's estimator of effect size and related estimators. *J. Educ. Stat.* 6, 107–128.
- Himberg, J., Hyvarinen, A., 2003. ICASSO: software for investigating the reliability of ICA estimates by clustering and visualization. In: *Neural Networks for Signal Processing - Proceedings of the IEEE Workshop*, pp. 259–268. <https://doi.org/10.1109/NNSP.2003.1318025>.
- Huffman, R.F., Henson, O.W., 1990. The descending auditory pathway and acousticomotor systems: connections with the inferior colliculus. *Brain Res. Rev.* 15, 295–323. [https://doi.org/10.1016/0165-0173\(90\)90005-9](https://doi.org/10.1016/0165-0173(90)90005-9).
- Hutchison, R.M., Leung, L.S., Mirsattari, S.M., Gati, J.S., Menon, R.S., Everling, S., 2011. Resting-state networks in the macaque at 7T. *NeuroImage* 56, 1546–1555. <https://doi.org/10.1016/j.neuroimage.2011.02.063>.
- Hutchison, R.M., Mirsattari, S.M., Jones, C.K., Gati, J.S., Leung, L.S., 2010. Functional networks in the anesthetized rat brain revealed by independent component analysis of resting-state fMRI. *J. Neurophysiol.* 103, 3398–3406. <https://doi.org/10.1152/jn.00141.2010>.
- Hutchison, R.M., Womelsdorf, T., Gati, J.S., Everling, S., Menon, R.S., 2013. Resting-state networks show dynamic functional connectivity in awake humans and anesthetized macaques. *Hum. Brain Mapp.* 34, 2154–2177. <https://doi.org/10.1002/hbm.22058>.
- Jafri, M.J., Pearlson, G.D., Stevens, M., Calhoun, V.D., 2008. A method for functional network connectivity among spatially independent resting-state components in schizophrenia. *NeuroImage* 39, 1666–1681. <https://doi.org/10.1016/j.neuroimage.2007.11.001>.
- Jürgens, U., Pratt, R., 1979. Role of the periaqueductal grey in vocal expression of emotion. *Brain Res.* 167, 367–378. [https://doi.org/10.1016/0006-8993\(79\)90830-8](https://doi.org/10.1016/0006-8993(79)90830-8).
- Kalia, B.M., Whitteridge, D., 1973. The visual areas in the splenic sulcus of the cat. *J. Physiol.* 232, 275–283.
- Karns, C.M., Dow, M.W., Neville, H.J., 2012. Altered cross-modal processing in the primary auditory cortex of congenitally deaf adults: a visual-somatosensory fMRI study with a double-flash illusion. *J. Neurosci.* 32, 9626–9638. <https://doi.org/10.1523/JNEUROSCI.6488-11.2012>.
- Klassen, L.M., Menon, R.S., 2004. Robust automated shimming technique using arbitrary mapping acquisition parameters (RASTAMAP). *Magn. Reson. Med.* 51, 881–887. <https://doi.org/10.1002/mrm.20094>.
- Kleine, J.F., Guan, Y., Buttner, U., 2003. Saccade-related neurons in the primate fastigial nucleus: what do they encode? *J. Neurophysiol.* 90, 3137–3154. <https://doi.org/10.1152/jn.00021.2003>.
- Knowlton, B.J., Thompson, J.K., Thompson, R.F., 1993. Projections from the auditory cortex to the pontine nuclei in the rabbit. *Behav. Brain Res.* 56, 23–30. [https://doi.org/10.1016/0166-4328\(93\)90019-M](https://doi.org/10.1016/0166-4328(93)90019-M).
- Kok, M.A., Chabot, N., Lomber, S.G., 2014. Cross-modal reorganization of cortical afferents to dorsal auditory cortex following early- and late-onset deafness. *J. Comp. Neurol.* 522, 654–675. <https://doi.org/10.1002/cne.23439>.
- Krauzlis, R.J., Goffart, L., Hafed, Z.M., 2017. Neuronal control of fixation and fixational eye movements. *Philos. Trans. R. Soc. B* 372. <https://doi.org/10.1098/rstb.2016.0205>.
- Kriegeskorte, N., Mur, M., Ruff, D.A., Kiani, R., Bodurka, J., Esteky, H., Tanaka, K., Bandettini, P.A., 2008. Matching categorical object representations in inferior

- temporal cortex of man and monkey. *Neuron* 60, 1126–1141. <https://doi.org/10.1016/j.neuron.2008.10.043>.
- Kyathanahally, S.P., Jia, H., Pustovoy, O.M., Waggoner, P., Beyers, R., Schumacher, J., Barrett, J., Morrison, E.E., Salibi, N., Denney, T.S., Vodyanov, V.J., Deshpande, G., 2015. Anterior-posterior dissociation of the default mode network in dogs. *Brain Struct. Funct.* 220, 1063–1076. <https://doi.org/10.1007/s00429-013-0700-x>.
- Leake, P.A., Hradek, G.T., Rebscher, S.J., Snyder, R.L., 1991. Chronic intracochlear electrical stimulation induces selective survival of spiral ganglion neurons in neonatally deafened cats. *Hear. Res.* 54, 251–271. [https://doi.org/10.1016/0378-5955\(91\)90120-X](https://doi.org/10.1016/0378-5955(91)90120-X).
- Lee, C.C., Winer, J.A., 2008. Connections of cat auditory cortex: III. Corticocortical system. *J. Comp. Neurol.* 507, 1920–1943. <https://doi.org/10.1002/cne.21613>.
- Lee, T.W., Girolami, M., Sejnowski, T.J., 1999. Independent component analysis using an extended infomax algorithm for mixed subgaussian and supergaussian sources. *Neural Comput.* 11, 417–441. <https://doi.org/10.1162/089976699300016719>.
- Liu, Y., Yu, C., Liang, M., Li, J., Tian, L., Zhou, Y., Qin, W., Li, K., Jiang, T., 2007. Whole brain functional connectivity in the early blind. *Brain* 130, 2085–2096. <https://doi.org/10.1093/brain/awm121>.
- Loe, P.R., Benevento, L.A., 1969. Auditory-visual interaction in single units in the orbito-insular cortex of the cat. *Electroencephalogr. Clin. Neurophysiol.* 26, 395–398.
- Lomber, S.G., Cornwell, P., Sun, J.S., MacNeil, M.A., Payne, B.R., 1994. Reversible inactivation of visual processing operations in middle suprasylvian cortex of the behaving cat. *Proc. Natl. Acad. Sci. U. S. A.* 91, 2999–3003. <https://doi.org/10.1073/pnas.91.8.2999>.
- Lomber, S.G., Malhotra, S., 2008. Double dissociation of “what” and “where” processing in auditory cortex. *Nat. Neurosci.* 11, 609–616. <https://doi.org/10.1038/nn.2108>.
- Lomber, S.G., Meredith, M.A., Kral, A., 2010. Cross-modal plasticity in specific auditory cortices underlies visual compensations in the deaf. *Nat. Neurosci.* 13, 1421–1427. <https://doi.org/10.1038/nn.2653>.
- Lomber, S.G., Payne, B.R., 2004. Cerebral areas mediating visual redirection of gaze: cooling deactivation of 15 loci in the cat. *J. Comp. Neurol.* 474, 190–208. <https://doi.org/10.1002/cne.20123>.
- Lomber, S.G., Payne, B.R., Cornwell, P., Long, K.D., 1996. Perceptual and cognitive visual functions of parietal and temporal cortices in the cat. *Cereb. Cortex* 6, 673–695. <https://doi.org/10.1093/cercor/6.5.673>.
- Lu, H., Zou, Q., Gu, H., Raichle, M.E., Stein, E.A., Yang, Y., 2012. Rat brains also have a default mode network. *Proc. Natl. Acad. Sci. U. S. A.* 109, 3979–3984. <https://doi.org/10.1073/pnas.1200506109>.
- Malhotra, S., Hall, A.J., Lomber, S.G., 2004. Cortical control of sound localization in the cat: unilateral cooling deactivation of 19 cerebral areas. *J. Neurophysiol.* 92, 1625–1643. <https://doi.org/10.1152/jn.01205.2003>.
- Malhotra, S., Lomber, S.G., 2007. Sound localization during homotopic and heterotopic bilateral cooling deactivation of primary and nonprimary auditory cortical areas in the cat. *J. Neurophysiol.* 97, 26–43. <https://doi.org/10.1152/jn.00720.2006>.
- Matsuyama, K., Drew, T., 1997. Organization of the projections from the pericruciate cortex to the pontomedullary brainstem of the cat: a study using the anterograde tracer Phaseolus vulgaris-Leucoagglutinin. *J. Comp. Neurol.* 389, 617–641.
- Meredith, M.A., Clemo, H.R., Corley, S.B., Chabot, N., Lomber, S.G., 2016. Cortical and thalamic connectivity of the auditory anterior ectosylvian cortex of early-deaf cats: implications for neural mechanisms of crossmodal plasticity. *Hear. Res.* 333, 25–36. <https://doi.org/10.1016/j.heares.2015.12.007>.
- Meredith, M.A., Kryklywy, J., McMillan, A.J., Malhotra, S., Lum-Tai, R., Lomber, S.G., 2011. Crossmodal reorganization in the early deaf switches sensory, but not behavioral roles of auditory cortex. *Proc. Natl. Acad. Sci. U. S. A.* 108, 8856–8861. <https://doi.org/10.1073/pnas.1018519108>.
- Musil, S., Olson, C., 1988. Organization of cortical and subcortical projections to anterior cingulate cortex in cat. *J. Comp. Neurol.* 272, 203–218.
- Musil, S.Y., Olson, C.R., 1993. The role of cat cingulate cortex in sensorimotor integration. In: *Neurobiology of Cingulate Cortex and Limbic Thalamus*, pp. 345–365. [https://doi.org/10.1007/978-1-4899-6704-6\\_12](https://doi.org/10.1007/978-1-4899-6704-6_12).
- Olson, C.R., Lawler, K., 1987. Cortical and subcortical afferent connections of a posterior division of feline area 7 (area 7p). *J. Comp. Neurol.* 259, 13–30. <https://doi.org/10.1002/cne.902590103>.
- Olulade, O.A., Koo, D.S., LaSasso, C.J., Eden, G.F., 2014. Neuroanatomical profiles of deafness in the context of native language experience. *J. Neurosci. Off. J. Soc. Neurosci.* 34, 5613–5620. <https://doi.org/10.1523/JNEUROSCI.3700-13.2014>.
- Penny, W.D., Friston, K.J., Ashburner, J.T., Kiebel, S.J., Nichols, T.E., 2011. *Statistical Parametric Mapping: the Analysis of Functional Brain Images*. Academic press.
- Popa, D., Popescu, A.T., Pare, D., 2009. Contrasting activity profile of two distributed cortical networks as a function of attentional demands. *J. Neurosci.* 29, 1191–1201. <https://doi.org/10.1523/JNEUROSCI.4867-08.2009>.
- Pujol, R., Marty, R., 1970. Postnatal maturation in the cochlea of the cat. *J. Comp. Neurol.* 139, 115–125.
- Raichle, M.E., MacLeod, A.M., Snyder, A.Z., Powers, W.J., Gusnard, D.A., Shulman, G.L., 2001. A default mode of brain function. *Proc. Natl. Acad. Sci. U. S. A.* 98, 676–682. <https://doi.org/10.1073/pnas.98.2.676>.
- Ron, S., Robinson, D.A., 1972. Eye movements cerebellar evoked by in the alert monkey stimulation. *Vis. Res.* 12, 1795–1808. [https://doi.org/10.1016/0042-6989\(72\)90070-3](https://doi.org/10.1016/0042-6989(72)90070-3).
- Rosell, A., Giménez-Amaya, J.M., 1999. Anatomical re-evaluation of the corticostriatal projections to the caudate nucleus: a retrograde labeling study in the cat. *Neurosci. Res.* 34, 257–269. [https://doi.org/10.1016/S0168-0102\(99\)00060-7](https://doi.org/10.1016/S0168-0102(99)00060-7).
- Royce, G.J., 1978. Cells of origin of subcortical afferents to the caudate nucleus: a horseradish peroxidase study in the cat. *Brain Res.* 153, 465–475.
- Shiell, M.M., Champoux, F., Zatorre, R.J., 2014. Enhancement of visual motion detection thresholds in early deaf people. *PLoS One* 9, e90498. <https://doi.org/10.1371/journal.pone.0090498>.
- Shipley, C., Buchwald, J.S., Carterette, E.C., Retardation, M., Angeles, L., 1988. The role of auditory feedback in the vocalization of cats. *Exp. Brain Res.* 431–438.
- Smith, S.M., Fox, P.T., Miller, K.L., Glahn, D.C., Fox, P.M., Mackay, C.E., Filippini, N., Watkins, K.E., Toro, R., Laird, A.R., Beckmann, C.F., 2009. Correspondence of the brain's functional architecture during activation and rest. *Proc. Natl. Acad. Sci. U. S. A.* 106, 13040–13045. <https://doi.org/10.1073/pnas.0905267106>.
- Snider, R.A.Y.S., York, N., 1966. Modification of cerebellar auditory responses by stimulation. *Exp. Neurol.* 200, 191–200.
- Snider, R.S., Stowell, A., 1944. Receiving areas of the tactile, auditory and visual systems in the cerebellum. *J. Neurophysiol.* 7, 331–657.
- Stolzberg, D., Wong, C., Butler, B.E., Lomber, S.G., 2017. Atlas: an MRI-based three-dimensional cortical atlas and tissue probability maps for the domestic cat (*Felis catus*). *J. Comp. Neurol.* <https://doi.org/10.1002/cne.24271>.
- Upadhyay, J., Baker, S.J., Chandran, P., Miller, L., Lee, Y., Marek, G.J., Sakoglu, U., Chin, C.L., Luo, F., Fox, G.B., Day, M., 2011. Default-mode-like network activation in awake rodents. *PLoS One* 6. <https://doi.org/10.1371/journal.pone.0027839>.
- Updyke, B., 1986. Retinotopic organization within the cat's posterior suprasylvian sulcus and gyrus. *J. Comp. Neurol.* 246, 265–280. <https://doi.org/10.1002/cne.902460210>.
- Vann, S.D., Aggleton, J.P., Maguire, E.A., 2009. What does the retrosplenial cortex do? *Nat. Rev. Neurosci.* 10, 792–802. <https://doi.org/10.1038/nrn2733>.
- Vincent, J.L., Patel, G.H., Fox, M.D., Snyder, A.Z., Baker, J.T., Van Essen, D.C., Zempel, J.M., Snyder, L.H., Corbetta, M., Raichle, M.E., 2007. Intrinsic functional architecture in the anaesthetized monkey brain. *Nature* 447, 83–86. <https://doi.org/10.1038/nature05758>.
- Walsh, E.J., McGee, J., Javel, E., 1986a. Development of auditory-evoked potentials in the cat. I. Onset of response and development of sensitivity. *J. Acoust. Soc. Am.* 79, 712–724. <https://doi.org/10.1121/1.393462>.
- Walsh, E.J., McGee, J., Javel, E., 1986b. Development of auditory-evoked potentials in the cat. II. Wave latencies. *J. Acoust. Soc. Am.* 79, 725–744. <https://doi.org/10.1121/1.393462>.
- Walsh, E.J., McGee, J., Javel, E., 1986c. Development of auditory-evoked potentials in the cat. III. Wave amplitudes. *J. Acoust. Soc. Am.* 79, 745–754. <https://doi.org/10.1121/1.393462>.
- Whitfield-Gabrieli, S., Nieto-Castanon, A., 2012. Conn: a functional connectivity toolbox for correlated and anticorrelated brain networks. *Brain Connect.* 2, 125–141. <https://doi.org/10.1089/brain.2012.0073>.
- Wong, C., Chabot, N., Kok, M.A., Lomber, S.G., 2015. Amplified somatosensory and visual cortical projections to a core auditory area, the anterior auditory field, following early- and late-onset deafness. *J. Comp. Neurol.* 523, 1925–1947. <https://doi.org/10.1002/cne.23771>.
- Xu, S.A., Shepherd, R.K., Chen, Y., Clark, G.M., 1993. Profound hearing loss in the cat following the single co-administration of kanamycin and ethacrynic acid. *Hear. Res.* 70, 205–215. [https://doi.org/10.1016/0378-5955\(93\)90159-X](https://doi.org/10.1016/0378-5955(93)90159-X).
- Zhou, Z.C., Salzwedel, A.P., Radtke-Schuller, S., Li, Y., Sellers, K.K., Gilmore, J.H., Shih, Y.-Y., Fröhlich, F., Gao, W., 2016. Resting state network topology of the ferret brain. *NeuroImage* 143, 70–81. <https://doi.org/10.1016/j.neuroimage.2016.09.003>.
- Zingg, B., Chou, X.L., Zhang, Z.G., Mesik, L., Liang, F., Tao, H.W., Zhang, L.L., 2017. AAV-mediated anterograde trans synaptic tagging: mapping corticocollicular input-defined neural pathways for defense behaviors. *Neuron* 93 (1), 33–47. <https://doi.org/10.1016/j.neuron.2016.11.045>.